

L1CAM-SECRETING CELLS AS PATHFINDERS FOR GLIOBLASTOMA

by

Alexander Stubbolo

A thesis submitted to the Faculty of the University of Delaware in partial fulfillment of the requirements for the degree of Honors Bachelor of Arts in Biological Sciences with Distinction

Spring 2018

© 2018 Alexander Stubbolo
All Rights Reserved

L1CAM-SECRETING CELLS AS PATHFINDERS FOR GLIOBLASTOMA

by

Alexander Stubbolo

Approved: _____
Deni Galileo, Ph.D.
Professor in charge of thesis on behalf of the Advisory Committee

Approved: _____
John McDonald, Ph.D.
Committee member from the Department of Biological Sciences

Approved: _____
Anna Klintsova, Ph.D.
Committee member from the Board of Senior Thesis Readers

Approved: _____
Paul Laux, Ph.D.
Director, University Honors Program

ACKNOWLEDGMENTS

I would like to thank the University of Delaware's Undergraduate Research Program; my fellow undergraduates Kyle Plusch, Camryn Bernheimer, and Michaela Scanlon; and graduate student Reetika Dutt. I would also like to thank my thesis committee for their help and guidance on this undertaking, along with all my professors at the University of Delaware who have been my mentors and my friends. Finally, I would like to thank my parents, Garth and Gwen Stubbolo for their continual support in all that I do.

TABLE OF CONTENTS

LIST OF FIGURES	vi
ABSTRACT	ix
1 INTRODUCTION	1
2 METHODS AND MATERIALS	5
2.1 Cell Lines.....	5
2.2 Time-Lapse Microscopy.....	6
2.3 Velocity Analysis	6
2.4 Chemotaxis Assays.....	7
2.5 Cell Motility and Chemotaxis Analysis	9
2.6 Statistics.....	10
2.7 <i>In vivo</i> Model: Chick Optic Tectum.....	10
2.8 Immunostaining protocol for L1 in tissue sections	11
2.9 Confocal Fluorescence Imaging	12
3 RESULTS.....	14
3.1 Cell Motility Analysis <i>in vitro</i>	14
3.2 Chemotaxis Analysis: Quantifying Directional Movement <i>in vitro</i>	18
3.3 <i>In vivo</i> Results	29
4 DISCUSSION.....	33
REFERENCES	37
A TRIAL AND ERROR IN DEVELOPING PROTOCOLS	41
A.1 Chemotaxis Assay Prototypes	41
A.1.1 Chemotaxis Plate Version 1 “The Double Ring”	41
A.1.2 Chemotaxis Plate Version 2 “Diamond of Rings”	43
A.1.3 Chemotaxis Plate Version 3 “The Krillin Plate”	44
A.1.4 <i>In vitro</i> images Used.....	45
A.2 <i>In vivo</i> Design.....	46

A.2.1	Vital dyes vs. viral labeling	46
A.2.2	Slide construction version 1	46
A.2.3	<i>In vitro</i> images used.....	48

LIST OF FIGURES

- Figure 1: Diagram of membrane-bound L1 and soluble L1 that is proteolyzed due to ADAM10 cleavage..... 2
- Figure 2: Diagram of “stripe assay” experimental setup. L1-negative cells were plated near a stripe of immobilized human immunoglobulin fragment, consisting of either IgG-Fc or L1-Fc, and tracked with time-lapse microscopy as they moved along the stripe..... 15
- Figure 3: Results of stripe assay. GBM cells tracked along stripe of immobilized L1 moved, on average, 50% faster than when moving along normal IgG-Fc. SEM <0.01..... 16
- Figure 4: Experimental setup for velocity analysis of mixed cell populations. Varying concentrations of GBM cell lines U-118/L1LE, U-118/1879, and fluorescently labeled U-118/1879 were plated, and fluorescent cells were tracked along the scratch edge indicated by the dotted line. The leftmost column, including the region containing the 25% L1LE vs 75% 1879+DiI and the region containing 25% 1879 vs 75% 1879+DiI evaporated and were not able to be tracked. Because this was a pilot experiment, based off of Anderson and Galileo’s results (2016) it was not repeated. 17
- Figure 5: Results for *in vitro* velocity analysis of U-118/1879 cells when mixed with different amounts of U-118/L1LE cells. Data was analyzed using a one-way ANOVA and found to have a *p* value <0.001; therefore the cells tracked in regions rich with L1 moved significantly faster than cells with no L1 present. SEM <0.01. 18
- Figure 6: Diagram of a modified chemotaxis assay plate with isolated cell populations. For experimental trials, regions 1,2) U-118/L1LE (L1-positive); 3-6) U-118/1879 (L1-negative). For control trials, all six regions would have the L1- negative cell type U-118/1879. Arrows indicate regions tracked and the observed movement of cells under experimental conditions. Not drawn to scale. 20

Figure 7a: This graph shows the average cell movement at each region along the Y-axis for control trials without regions of L1-secreting cells present. Red bars indicate regions with average Y-movement in the negative range (net movement downward). The scale has been modified to more explicitly show the pattern of movement present in control trials. Error bars are +/- 1 SEM. 21

Figure 7b: This figure shows the same information as is present in Figure 7a, scaled to match Figure 8 for a better comparison between the magnitude of difference between control and experimental trials. Error bars are +/- 1 SEM. 22

Figure 8: This graph shows the average cell movement along the Y-axis for each region of experimental trials, where L1-secreting cells are present. Positive values are taken to represent movement upwards, toward regions of high L1. Red bars indicate regions with average Y-movement in the negative range (net movement downward) Error bars are +/- 1 SEM. 23

Figure 9a: The summed Y-movement value designated for all regions for each experimental condition (with L1-secreting cells vs without L1-secreting cells) were averaged. This graph compares the average of all regions' summed Y-movement between control and experimental conditions. The average shows a dramatic increase in positive movement in cells tracked in the presence of L1-secreting cells. Control SEM = +/- 64; Experimental SEM = +/- 51. 24

Figure 9b: In the presence of L1-secreting cells, L1-negative cells moved an average of 33% faster than cells that were not exposed to L1ecto. P-value >0.05, error bars are +/- 1 SEM. 25

Figure 10: U-118/1879 cells along edge of bounded growth area. Control setup with no L1 secreting cells present. Image from time-point 1, with red lines indicating the path of cell movement over 22 hours. 26

Figure 11: U-118/1879 cells along edge of bounded growth area. Experimental setup with L1 secreting cells present, grown vertically above the shown region. Image from time-point 1, with red lines indicating the path of cell movement over 22 hours. 27

Figure 12a: Maximum projections of fluorescently labeled cells from a confocal z-stack of *In vivo* model control trial images. Chick brains were injected with a mixture of the same L1-negative GBM cell type, labelled with two different colors. Maximum projections of fluorescently labeled cells in a confocal z-stack. Virally labeled U-118/1879/mCherry (red), and U-118/1879/GFP (green). **A-C** imaged at 20x, **D** imaged at 10x..... 30

Figure 12b: Maximum projections of fluorescently labeled cells from a confocal z-stack of *In vivo* images under experimental conditions; mixture of L1-positive (red), and L1-negative (green) cells. Virally labeled U-118/L1LE/mCherry (red), U-118/1879/GFP (green), and immunostained L1 (blue). **A-C** imaged at 20x, **D** imaged at 10x. 31

Figure 13: First attempt at designing a modified chemotaxis assay plate. L1-negative cells were grown in outer region of plate, while L1-secreting cells were grown for 24 hours inside the bounded inner circle created from adhering the mouth of a 15mL plastic tube with rubber cement. Once removed, the area where the tube had been became the space where responding cells' movement was tracked with time-lapse microscopy. 42

Figure 14: The second chemotaxis plate prototype involved using rubber cement to adhere four plastic rings in a diamond-shape pattern. No cells were grown in what would be considered "the outer ring" in the previous experimental setup. Arrows indicate the potential movement of cells.... 44

Figure 15: The penultimate experimental design for the chemotaxis plate; pilot experiments using this design yielded encouraging results, but I decided that having a square border would be more consistent. 45

Figure 16: The first version of my slides for mounting 350-micron tissue sections. This design was effective for preventing tissue sections from being crushed, but it was impossible to seal with nail polish which prevented preservation of the slides for future use. 47

Figure 17: The second iteration of my slide design for mounting 350-micron tissue sections. By having the entire area around the specimen elevated with electrical tape, I was able to seal the cover glass with nail polish in order to preserve the slide for future use. 48

ABSTRACT

Purpose

Glioblastoma multiforme is one of the most common and most malignant forms of brain cancer. Part of what makes this kind of cancer so dangerous is the tendency for tumors to regrow and kill patients after initial tumor removal. Currently, there is no definitive treatment for such cases, nor is there a consensus on the cause. It is hypothesized that part of the cause is the abnormal presence of L1, a cell adhesion molecule. Previous studies have shown that upregulation of L1 increases motility and proliferation in glioblastoma cells. Here, I further investigated the effect of L1's presence on cancer motility and proliferation, as well as a possible chemotactic relationship that suggests a leader-follower relationship between sources of high L1 concentration and glioblastoma cells.

Methods

In vitro experiments utilizing time-lapse microscopy were used to quantify the velocity and directionality of migrating cancer cells, utilizing L1-positive and L1-negative variants of the human glioblastoma-derived, immortalized cell lines derived from U-118 MG. *In vivo* experiments used the same cells, with virally labeled fluorescent markers, injected into the optic tecta of developing chick embryos. The chicks' brains were allowed to develop until embryonic day 15, when they were dissected, fixed in paraformaldehyde, embedded in agar, and sectioned. The sections

of brain were immunostained and imaged using confocal microscopy to qualitatively determine relationships between L1-secreting cells and L1-negative cells.

Results

In vitro time-lapse microscopy experiments showed a significant increase in the velocity of migrating glioblastoma cells when sources of L1ecto were present, as well as a significant trend of directional movement toward regions of L1-secreting cells. *In vivo* chick model experiments showed L1-negative glioblastoma cells appearing to be closely coupled with L1-secreting cells as they moved through the developing brain of a fetal chick.

Conclusions

My results strengthen the argument that the abnormal expression of L1 in glioblastoma multiforme increases the motility and proliferation of glioblastoma cells, and also suggests that sources of L1ecto may guide the directional movement of glioblastoma cells, both *in vitro* and *in vivo*. This suggests cells that secrete soluble L1 may act as pathfinders for surrounding cancer cells. Potentially, these L1-positive cells could act as beacons for surrounding cancer cells to regroup around them to form new tumor masses after surgical resection. These findings emphasize the importance of researching molecular inhibitors of L1 as potential adjuvant therapies for brain cancer.

Chapter 1

INTRODUCTION

Chemotaxis is understood as the phenomenon of directed cell movement in response to a chemical gradient, and is important in innumerable physiological processes (Swaney, et al., 2010). Normal chemotaxis can be observed in the recruitment of inflammatory cells to infected sites, organ development, and other vital processes (Roussos, et al., 2011). However, abnormal chemotaxis is often present in many forms of cancer. Normal chemotaxis pathways can be “hijacked” by cancer cells to aid in metastasis (Condeelis, et al., 2005). Chemotactic effects have been studied in several pathways, including the cofilin (Wang et al., 2007) pathway as well as several chemokine pathways (Koshiba et al., 2000; Scotton et al., 2002), along with many others. Until now, there has been no evidence to suggest that the L1 signaling pathway is involved in chemotaxis.

L1CAM (also known as L1; CD171; etc.) is a member of the immunoglobulin (Ig) superfamily, and acts as a transmembrane glycoprotein (Faissner et al., 1985; Moos et al., 1988). L1 is vital for the development of the nervous system as it is present in neural cell adhesion (Keilhauer, et al., 1985), cell survival, and cell proliferation processes (Conacci-Sorrell et al., 2005). Of particular interest to this paper is L1’s involvement in neuronal migration and axonal outgrowth (Anderson & Galileo, 2016; Chang, et al., 1987; Lindner, et al., 1983).

L1 is active as a cell surface molecule, but it can also be proteolyzed by ADAM10 cleavage which releases L1 as soluble ectodomain (Maretzky et al., 2005).

Normally, L1 is present as a complete transmembrane protein in the adult brain (Liljelund, et al., 1994), but many types of cancers can cause unregulated ADAM10 cleavage (Fig. 1). This leads to a large amount of soluble L1 ectodomain (L1ecto) that acts on cancer cell surface receptors in a paracrine/autocrine manner and increases the motility and proliferation of the cancer – heightening the cancer’s invasiveness and ability to metastasize (Gutwein et al., 2003; Kiefel et al., 2012). One kind of cancer that L1 is expressed abnormally in is glioblastoma multiforme (GBM).

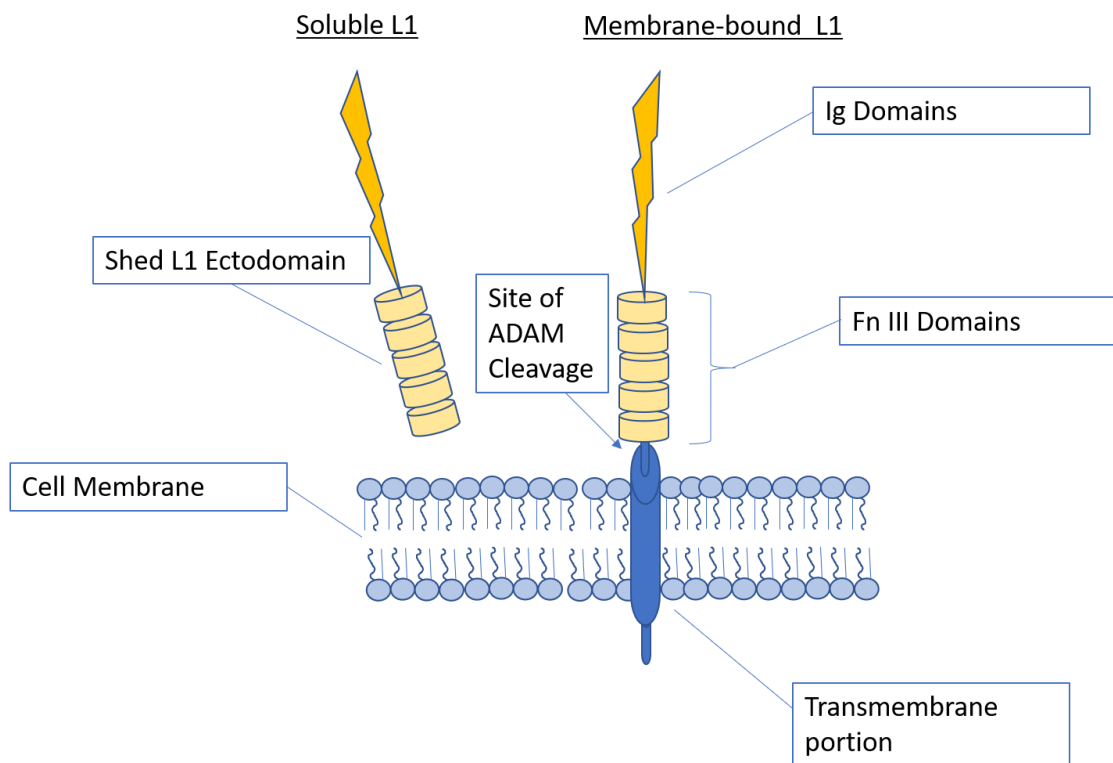


Figure 1: Diagram of membrane-bound L1 and soluble L1 that is proteolyzed due to ADAM10 cleavage.

GBM is the most common and most lethal type of brain cancer in adult humans (Wen and Kesari, 2008), known for its extreme invasiveness (De Bonis et al., 2013). After the standard treatment of maximal safe surgery and adjuvant chemo- and radio-therapy, most patients experience a recurrence after six to nine months of primary treatment (Mallick et al., 2016). Because advances in the standard treatment of GBM have not greatly improved the mortality rate of affected patients in the last several decades (Smoll et al., 2013), interest has turned to developing molecular treatment options and understanding the nature of GBM's invasiveness. Previous research has shown that the presence of soluble L1 increases GBM's motility, proliferation, and invasiveness by acting on integrin, focal adhesion kinase (FAK), and fibroblast growth factor receptor (FGFR) signaling pathways (Anderson and Galileo, 2016; Mohanan, et al., 2013; Yang et al., 2011).

Anderson and Galileo (2016) showed that the presence of L1 stimulated cancer cells to increase their velocity *in vitro* while they investigated the effects of FAK small molecule inhibitors. This paper corroborates that L1 increases the motility of cancer cells *in vivo*.

This research aimed to discern whether the molecule L1 can act as a chemoattractant for glioblastoma cells and affect not only the motility and proliferation of cancer cells, but also their directional movement. To this end, I aimed to develop a reliable, accurate, and reproducible *in vitro* assay to determine chemotactic movement in migrating cells using inexpensive laboratory materials and time-lapse microscopy. I also aimed to examine the relationship between glioblastoma cells that secrete L1 and those that do not within the *in vivo* model of developing chicken brain tissue.

Here, I have also shown that L1-negative cells tend to migrate directionally toward sources L1ecto concentration both *in vivo* and *in vitro*. This may help to elucidate the pattern of cancer behavior that causes tumors to often regrow after surgical resection and inform research into molecular inhibitors of L1 signaling as possible avenues for adjuvant therapy for cancer patients.

Chapter 2

METHODS AND MATERIALS

2.1 Cell Lines

The same cell lines and culture conditions were used as described by Anderson and Galileo (2016). U-118 MG (Ponten and Westermarck, 1978) is a human glioblastoma-derived cell line that was obtained from the American Type Culture Collection (ATCC, Manassas, VA). The cells were cultured in Dulbecco's Modified Eagle Medium (DMEM, Thermo Fisher Scientific) with 10% fetal bovine serum (FBS), 2mM L-glutamine, and 100 microgram/ml penicillin-streptomycin (referred to here as "complete DMEM"). The cells were incubated at 37 °C with 5% CO₂. It has been previously shown that U-118 cells do not typically express soluble L1 protein (Yang et al., 2011). The U-118 cells were transduced with a lentiviral vector K1879/L1LE to encode the L1 long ectodomain (L1LE) to create the L1-secreting form U-118/L1LE cells (Mohan et al., 2013). To contrast these, L1-negative control cells were made by transducing U-118 cells with an empty K1879 vector (U-118/1879). These modified cell lines were used for the *in vitro* and *in vivo* experimental models described forthwith. From here on out, "L1-secreting cells" and "L1 – positive cells" refer to the transduced U-118/L1LE cells, while "L1-negative cells" refers to the U-118/1879 cells for ease of reference. Furthermore, the soluble, proteolyzed ectodomain of the L1CAM gene product will be referred to as "L1 ecto" or "soluble L1."

2.2 Time-Lapse Microscopy

Time-lapse microscopy was performed on an imaging system that was originally described by Fotos et al. (2006). *In vitro* assays were performed by growing cells in bounded regions on custom cell culture plates, and imaging migrating cells with time-lapse microscopy, utilizing a customized incubator. The incubator was built on an adjustable ProScan II automated stage (Prior Scientific, Rockland MA). The cells were maintained at atmospheric conditions of 5% CO₂ to 95% air and 37 °C using a gas injection controller (Forma Scientific, Marietta, OH), a warm air temperature controller (Air Therm, World Precision Instruments, Sarasota FL), and a temperature-controlled stage insert (Tokai Hit, Shizuoka-ken, Japan). The cells were photographed using a CoolSnap ES CCD camera (Photometrics, Tucson, AZ) or a RetigaEXi Fast camera (QImaging, Surrey, British Columbia) and a 10x Nikon Plan Fluor objective. The system was controlled by MetaMorph Software (Version 7.8.12.0; Molecular Devices Corporation, Downingtown, PA). Tracking of cells was performed using the “Track Points” application for the same version of MetaMorph.

2.3 Velocity Analysis

Before experimenting to determine the effect of L1 on the directional movement of glioblastoma multiforme cells, I followed up on the results of Anderson and Galileo to examine stimulatory effect of L1 on the motility of GBM cells. To analyze the effect of L1-secreting cells on GBM cell velocity, a motility assay was performed wherein a stripe of chimeric human L1-Fc (R&D Systems, Minneapolis MN; Catalog #10702-HNAH) was immobilized on a cell culture dish and L1-negative

cells were seeded alongside it. Cells were tracked with time-lapse microscopy as they moved along the stripe. (See Fig. 2 in Results section). This was compared to a control experiment wherein cells were seeded alongside a stripe of immobilized chimeric human IgG-Fc (Sino Biological Inc., North Wales PA; Catalog #777-nc).

To further demonstrate the velocity-stimulating effects of L1, a six-well cell culture plate was seeded with differing concentrations of U-118/1879 and U-118/L1LE cells, as well as U-118/1879 cells stained with Vybrant DiI vital dye (Thermo Fisher Scientific, Waltham MA; Catalog #V22885). After 24 hours of growth, a scratch edge was made with a P1000 soft plastic micropipette tip, and individual cells at the scratch edge were tracked for 22 hours using MetaMorph software. Fluorescence illumination was used to locate and track labeled U-118/1879 cells along the scratch edge. The conditions were 25% U-118/1879/DiI and 75% U-118/L1LE; 50% U-118/1879/DiI and 50% U-118/L1LE; and 75% U-118/1879/DiI and 25% L1LE. The control conditions included the same concentrations of U-118/1879/DiI but set against U-118/1879 cells without DiI (See Fig. 4 in Results section).

2.4 Chemotaxis Assays

To analyze the chemotactic effect of L1 on the directional movement of glioblastoma cells, custom cell culture dishes were used (See Fig 6 in Results section). The plates were overlaid with a hydrophobic, adhesive tape (Patco 5865 Heavy-Duty Removable Protective Film Tape; 2 in. width; FindTape.com) mask with six 1cm square regions cut out for cells to grow. There were multiple iterations of design

prototypes for this customized cell culture plate; for a description of the previous models, see Appendix A. The plate with tape mask was then sterilized for 30 minutes with an ultraviolet transilluminator before cell culture. Approximately 4×10^5 cells were seeded onto each of the bounded regions and allowed to grow in complete DMEM for several hours. Once the cells had attached to the dish and spread out (viewable via phase contrast microscopy) the media was aspirated off and the cells were rinsed with phosphate buffered saline (PBS). The bounding tape mask was carefully removed with sterilized forceps, and 8mL of complete DMEM containing 1.25% methyl cellulose was slowly added to the dish. Methyl cellulose was added into the complete media to thicken it as a means of further preserving a gradient of L1ecto. The dish was placed into the time-lapse incubator for one hour before imaging began to allow time for the cells to settle in the new media.

Experimental plates contained U-118/L1LE cells seeded on the top two regions (regions 1 and 2 in Fig. 6) and U-118/1879 cells seeded onto the bottom four regions (regions 3,4,5, and 6 in Fig. 6). Control plates, in contrast, had U-118/1879 cells grown in all six regions. In all time-lapse trials – both experimental and control – vertical regions along the sides of regions 3-6 were imaged every 10 minutes for 22 hours. Tracked regions of cells were chosen randomly. Five experimental trials were successfully performed, and four control trials were successfully performed; out of those trials, which were performed under the same experimental conditions, each random region of 15 tracked cells was considered to be one experimental region. More experimental and control trials were attempted, but due to a recurrence of camera

timeout issues, many had to be prematurely terminated. Also worthy of note is that not all regions selected for imaging were used if the view became obscured over the course of the experiment, or if large areas of cells detached due to growing beyond confluency.

2.5 Cell Motility and Chemotaxis Analysis

For every *in vitro* experiment that utilized time-lapse microscopy, MetaMorph software was used to analyze the movement of cells. Images were manually renamed to contain a sequential three-digit naming value, and the resultant stack of images for each trial was compiled and exported to MetaMorph. The Track Points application was used to manually track the movement of each cell as it migrated over time. Fifteen cells were chosen out of the population viewable at each region and tracked. The tracked cells were chosen and marked at the first timepoint so that the person tracking the cell would not know where the cell's movement would stop. If, over the course of the experiment, a selected cell underwent mitosis, only one of the daughter cells was tracked. The rule of thumb used was to choose the daughter cell furthest to the horizontal left; this distinction was chosen arbitrarily. All the tracked cells' movement data was exported to a Microsoft Excel spreadsheet, including each cell's change in position along the X and Y axes. From this data, the mean cell velocities, as well as the mean, and summed directional movement of the cells were determined. The efficacy of this software has been shown by Fotos et al. (2006) and Anderson and Galileo (2016) for the purpose of determining cell velocity under a given condition.

2.6 Statistics

Paired t-tests, Student's t-test, and one-way ANOVA were used when appropriate to analyze the data. A p value of 0.05 was chosen as the cutoff to determine a significant result.

2.7 *In vivo* Model: Chick Optic Tectum

The optic tectum of an embryonic chick was used as an *in vivo* model to examine the interaction of GBM cells with L1-producing and L1-negative cell lines. Preparations were the same as previously described (Cretu et al., 2005). We obtained Fertile White Leghorn chicken embryos from the University of Delaware Department of Animal and Food Sciences. The eggs were kept at 37.5°C in a humidified force-draft incubator until embryonic day 5 (E5) of development; E0 was designated as the day when the eggs were put into the incubator.

U-118/L1LE and U-118/1879 cells were virally labeled with fluorescent markers and injected into chick embryos at E5 of development. To inject the tumor cells, the eggs were sterilized with 70% ethanol and a small hole was cut with scissors over the air space at the blunt end of the egg. The inner membrane was wetted with a Medium 199 (Mediatech, Inc.) and removed with fine forceps. 5µL of the virally labeled, mixed cell suspension, containing approximately 5×10^5 cells, was microinjected with a PV830 pneumatic picopump (World Precision Instruments; Sarasota, FL). The suspension was injected into one of the midbrain ventricles in the embryonic chick's brain. After injection, a few drops of 50mg/mL sterile ampicillin were placed on top of the embryo, and clear adhesive tape was used to seal the hole in the shell.

The injected embryos were placed back into the incubator and allowed to grow for 10 days. At E15, the chick embryos were sacrificed and their optic tecta were dissected, fixed in 2% paraformaldehyde in 0.1M sodium cacodylate buffer, and embedded in a solidified solution of PBS with 8% sucrose and 3.5% agar for sectioning. The embedded tecta were then sectioned into 350-micron sections with a Vibratome model 3000 sectioning system and stored in PBS at 4°C until they were immunostained for L1 and mounted on slides for imaging.

2.8 Immunostaining protocol for L1 in tissue sections

To immunostain for the presence of soluble L1 molecules in tissue sections, I used a three-tier antibody staining technique that utilized biotin-avidin conjugated antibodies. 350-micron tissue sections were immersed in a solution of PBS with 0.1% Triton X-100 detergent, and 5% Normal Goat Serum (PBSTG) with a 1/100 concentration of Anti-L1CAM UJ127 primary monoclonal antibody (Santa Cruz Biotechnology, Catalog #53386). Sections were incubated for 24 hours at 4°C with constant, light agitation on an orbital shaker. Sections were then rinsed 3x for 1 hour each in PBSTG, followed by incubation in a solution of PBSTG with a 1/200 dilution of Biotin-conjugated goat anti-mouse IgG secondary antibody (Jackson ImmunoResearch Catalog #115-065-146). Sections were incubated for 20 hours at 4°C with constant agitation. Sections were rinsed 3x for 1 hour each in PBSTG. Afterwards, the sections were incubated in a solution of PBSTG with 1/500 dilution of Alexa 647-conjugated streptavidin (Jackson ImmunoResearch Catalog #016-600-084) for 20 hours, at 4°C with constant agitation. Sections were rinsed 3 x 1 hour each in

PBSTG before being mounted on slides in clearing mounting media with N-Propyl-Gallate (Acros Organics).

To allow for the thickness of the tissue sections during mounting, slides were masked with two layers of 170-micron thick (standard) electrical tape, with a 1cm square cut out of the middle to allow space of the specimen (See Fig. 16 in Appendix A). This allowed for a platform for the cover glass to rest on without crushing the tissue section. It also allowed for the cover glass to be sealed around its periphery with nail polish to prevent dehydration of the specimen without the problem of nail polish bleeding into the mounting media (See Appendix A).

2.9 Confocal Fluorescence Imaging

The 350-micron sections were imaged using a scanning laser confocal microscope, and the resultant stacks of images were rendered into 3-dimensional volume renders. The confocal microscope system consisted of a Nikon E800 upright microscope with Plan Apo objectives connected to a Nikon C1 scanning laser confocal microscope system. Lasers consisted of a 40mw 488nm (blue) Argon laser, a 1.4mw 543nm (green) HeNe laser, and a 14mw 633nm (red) HeNe laser. The E800 was equipped with a Nikon Remote Focus Accessory to allow precise z-stacks of images to be acquired. Nikon EZ-C1 software (ver. 3.94) was used to control the microscope, collect images, and produce maximum projections and volume renders of acquired z-stacks. Virally labeled green fluorescent protein (GFP) and red fluorescent protein (mCherry) were visualized in addition to the immunostained L1 molecules (far-red Alexa 647). As such, in the volume renders and the resultant maximal projections, the

fluorescently labeled glioblastoma cells as well as L1 molecules were visible (See Fig. 12 in Results section).

Chapter 3

Results

3.1 Cell Motility Analysis *in vitro*

Before beginning to analyze the effect of L1 on the directional movement of glioblastoma multiforme cells, I examined previous claims that L1 had a stimulatory effect on cancer cell motility in general (Anderson and Galileo, 2016). I studied the stimulatory effects of L1 with a number of *in vitro* time-lapse assays. Cell velocity in the presence of L1 was first examined using the aforementioned “stripe assay”, wherein cells were plated on and near a stripe of immobilized human IgG-Fc or human L1-Fc and tracked as they moved along the stripe (Fig. 2); a Student’s t-test analyzed the experimental and control velocities and showed that cells moved significantly faster on immobilized L1-Fc than on immobilized IgG-Fc. (Fig 3).

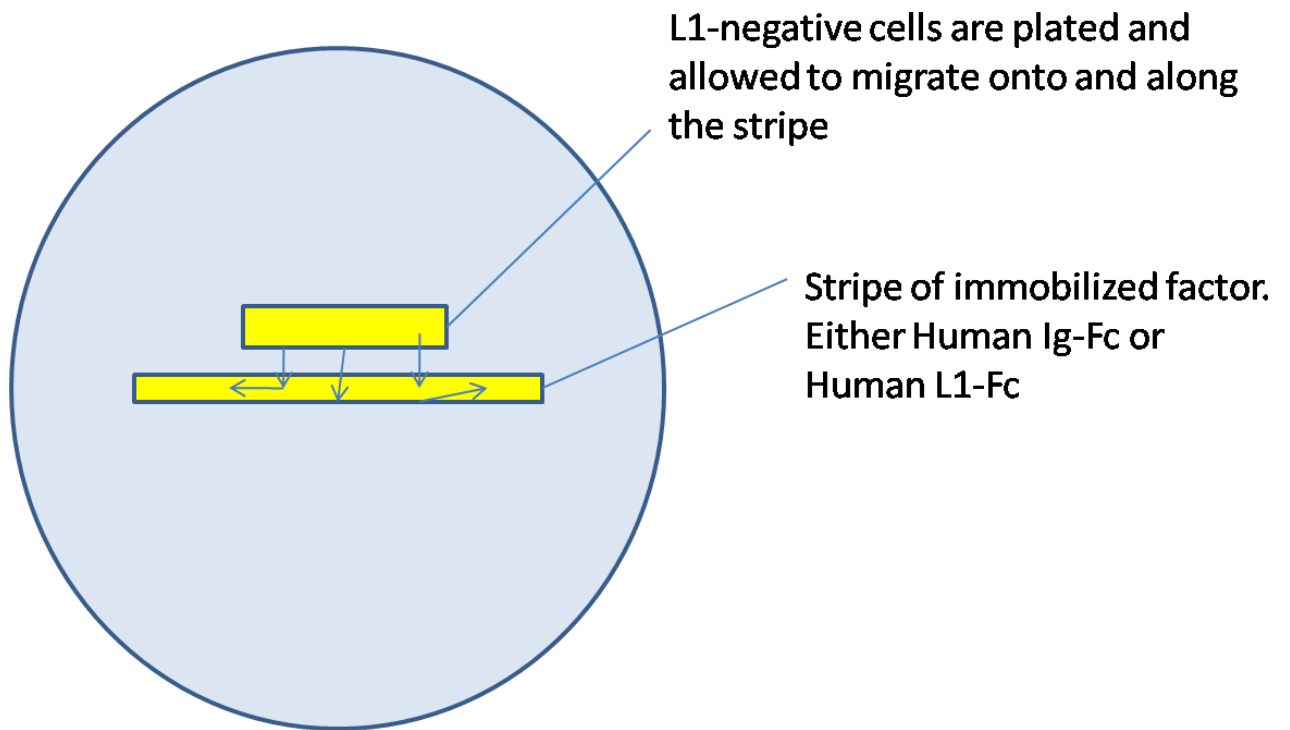


Figure 2: Diagram of “stripe assay” experimental setup. L1-negative cells were plated near a stripe of immobilized human immunoglobulin fragment, consisting of either IgG-Fc or L1-Fc, and tracked with time-lapse microscopy as they moved along the stripe.

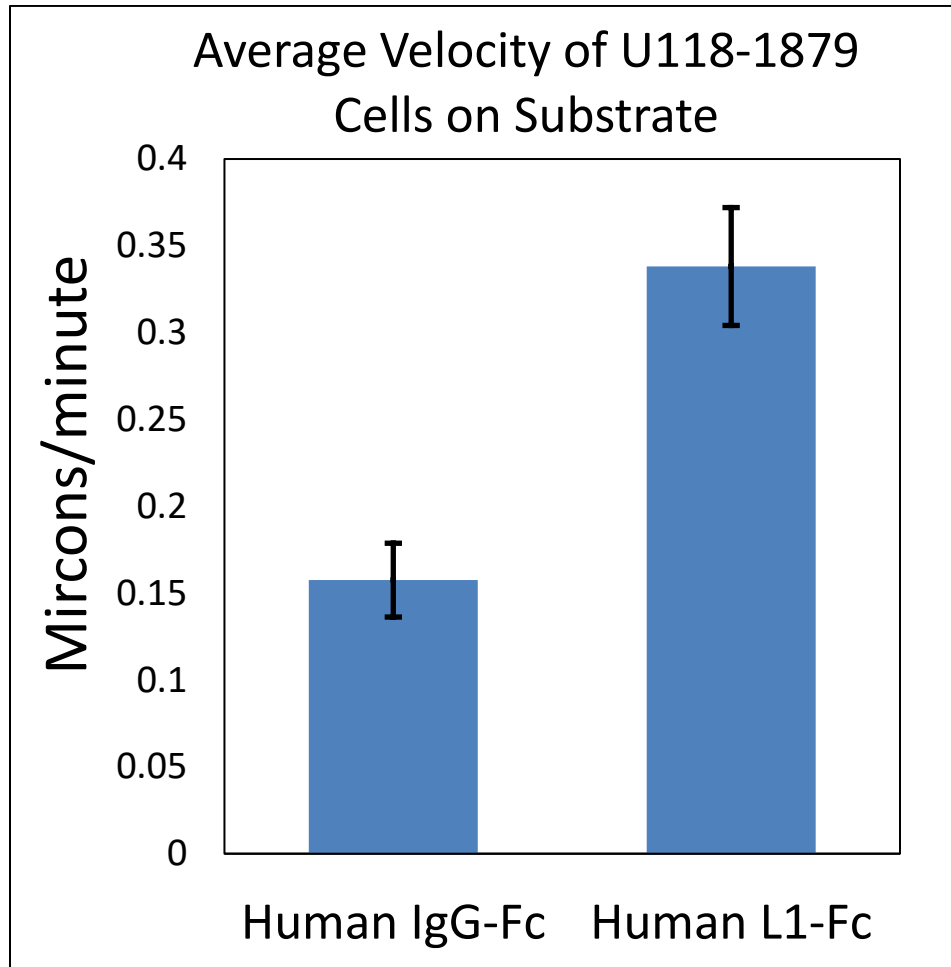


Figure 3: Results of stripe assay. GBM cells tracked along stripe of immobilized L1 moved, on average, 50% faster than when moving along normal IgG-Fc. SEM <0.01.

Another cell velocity analysis utilized mixed concentrations of cells in a six well cell culture plate, as described in the methods section. The velocities of cells were significantly greater when L1-secreting cells were present (Figs. 4 and 5). As I tracked cells that did not express their own L1 protein, their increased movement speed

indicated that these cells were being stimulated by L1-producing cells in a paracrine way. These experiments extended those of Anderson and Galileo (2016) and created incentive for analyzing the potential chemotactic effects of proteolyzed, soluble L1 on glioblastoma multiforme cell lines in an *in vitro* model.



Figure 4: Experimental setup for velocity analysis of mixed cell populations. Varying concentrations of GBM cell lines U-118/L1LE, U-118/1879, and fluorescently labeled U-118/1879 were plated, and fluorescent cells were tracked along the scratch edge indicated by the dotted line. The leftmost column, including the region containing the 25% L1LE vs 75% 1879+DiI and the region containing 25% 1879 vs 75% 1879+DiI evaporated and were not able to be tracked. Because this was a pilot experiment, based off of Anderson and Galileo's results (2016) it was not repeated.

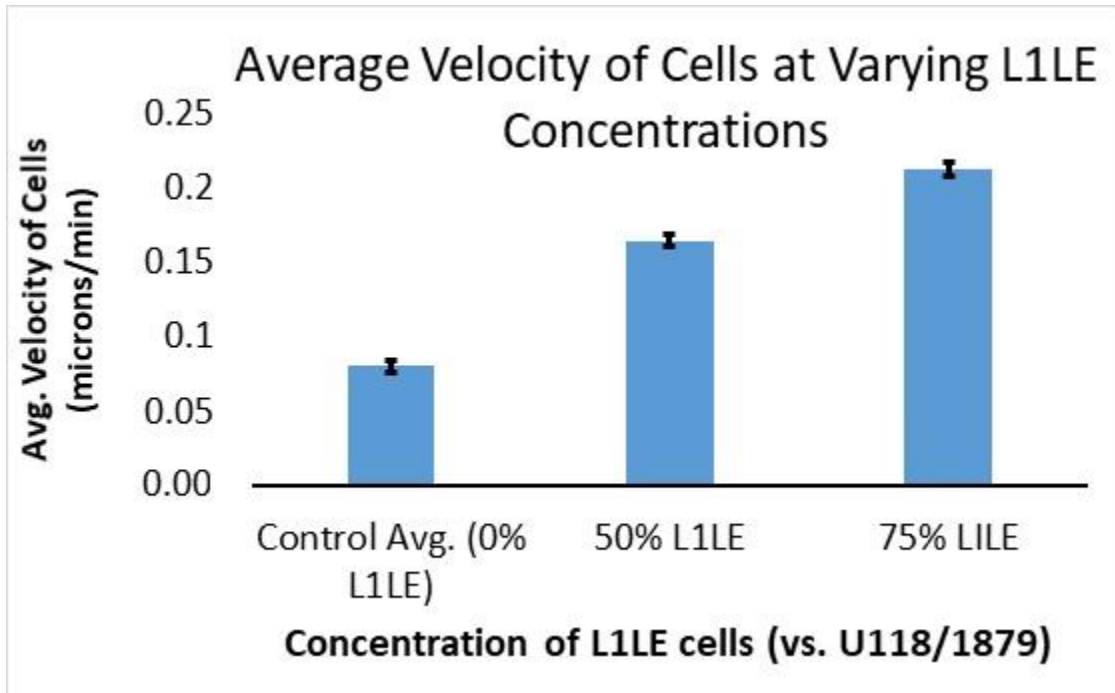


Figure 5: Results for *in vitro* velocity analysis of U-118/1879 cells when mixed with different amounts of U-118/L1LE cells. Data was analyzed using a one-way ANOVA and found to have a p value <0.001 ; therefore the cells tracked in regions rich with L1 moved significantly faster than cells with no L1 present. SEM <0.01 .

3.2 Chemotaxis Analysis: Quantifying Directional Movement *in vitro*

The bulk of this study's experiments were focused on determining if human GBM cells displayed preferential, directional movement toward regions of high soluble L1 concentration. Cells along a vertical flat edge were tracked with time-lapse microscopy and their movement along the Y-axis was recorded (Fig 6). Delta Y values were recorded at each time point, for each of the 15 cells tracked, per region. Any movement upward (toward the regions of L1-secreting GBM cells) would register as a positive value, while any movement downward (away from L1-secreting GBM cells) would register as a negative value.

Net delta Y values were determined for all 15 cells in each region, and the movement of all cells were averaged for each region. When performing statistical analysis or graphing the data, the average Y-movement for each *region* was counted as a single data point as the mean and SEM for the net delta Y is shown for each region in Fig. 7 and 8, and because the 15 cells within each region may not be statistically independent, the mean net delta Y for each region is considered as one data point for the one-sample t-test.

Summing the Y-movement for each cell was deemed most applicable because the minute-to-minute movement of glioma cells is highly erratic, and this research is most interested in the overall trends of cell movement. The assumption was that if there were no chemotactic effects from a source of soluble L1, all positive and negative movements of cells along the Y-axis would effectively cancel out and the net movement would not differ significantly from zero. Use of one-sample t-tests on the average movement of cells at each region showed that in control experiments, without regions of L1-secreting cells, directional movement did not differ significantly from zero (p-value = 0.61) while the experimental trials, with regions of L1-secreting cells, did differ significantly from zero (p-value <0.01). This suggests that GBM cells responded to chemotactic cues and preferentially moved directionally toward regions of high L1ecto concentration (Fig. 6, 7, 8).

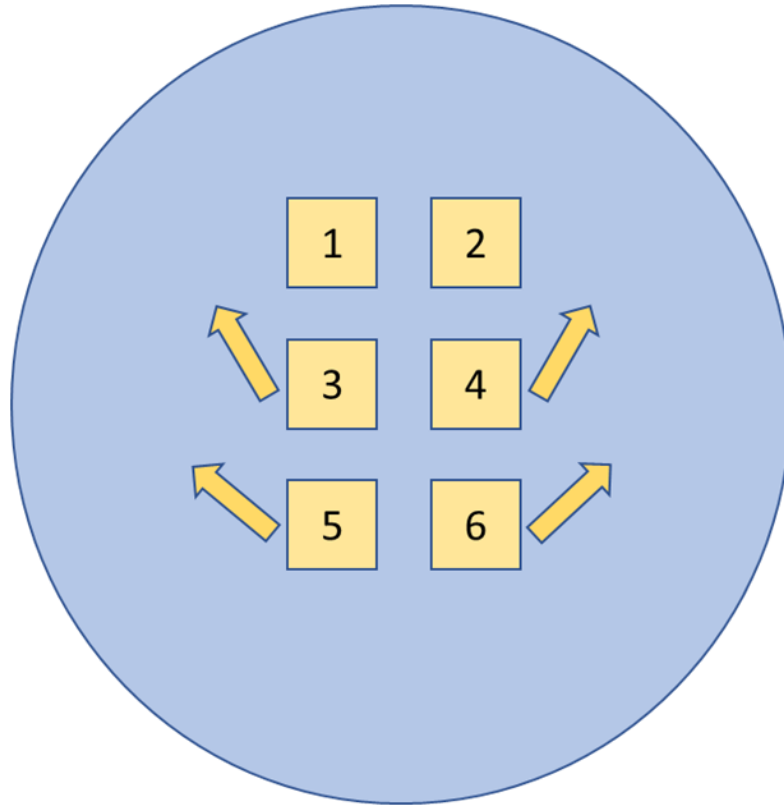


Figure 6: Diagram of a modified chemotaxis assay plate with isolated cell populations. For experimental trials, regions 1,2) U-118/L1LE (L1-positive); 3-6) U-118/1879 (L1-negative). For control trials, all six regions would have the L1- negative cell type U-118/1879. Arrows indicate regions tracked and the observed movement of cells under experimental conditions. Not drawn to scale.

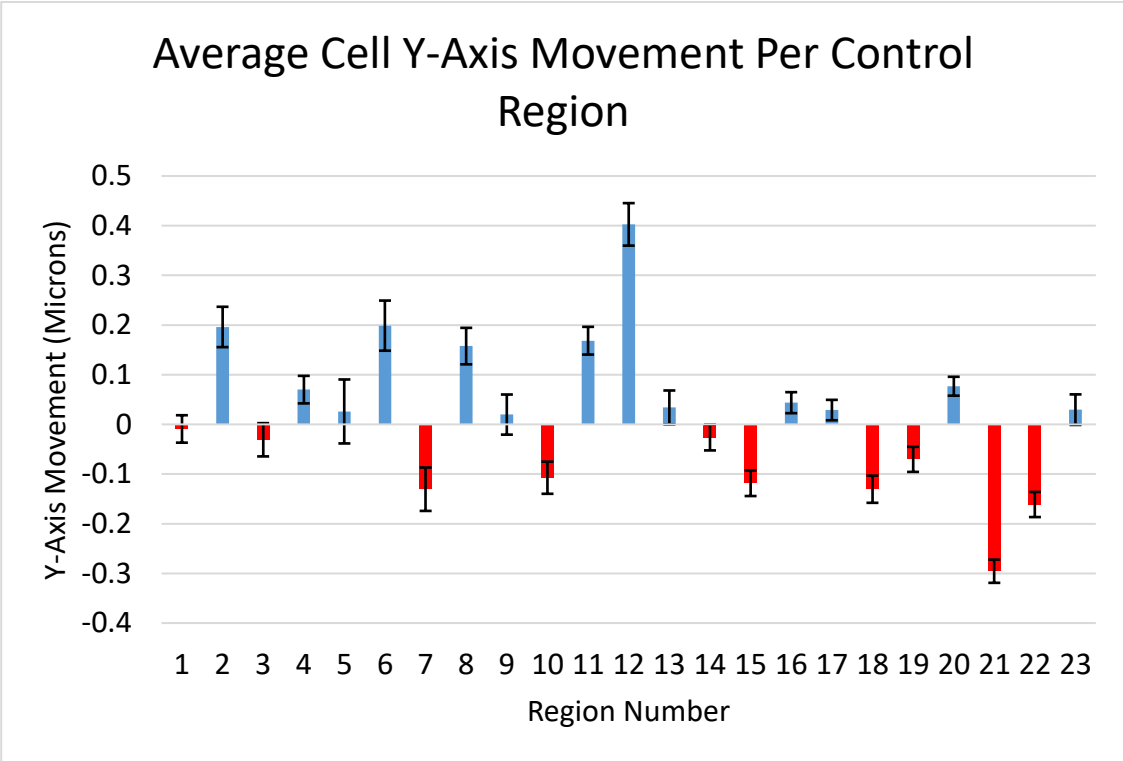


Figure 7a: This graph shows the average cell movement at each region along the Y-axis for control trials without regions of L1-secreting cells present. Red bars indicate regions with average Y-movement in the negative range (net movement downward). The scale has been modified to more explicitly show the pattern of movement present in control trials. Error bars are +/- 1 SEM.

Average Cell Y-Axis Movement Per Control Region

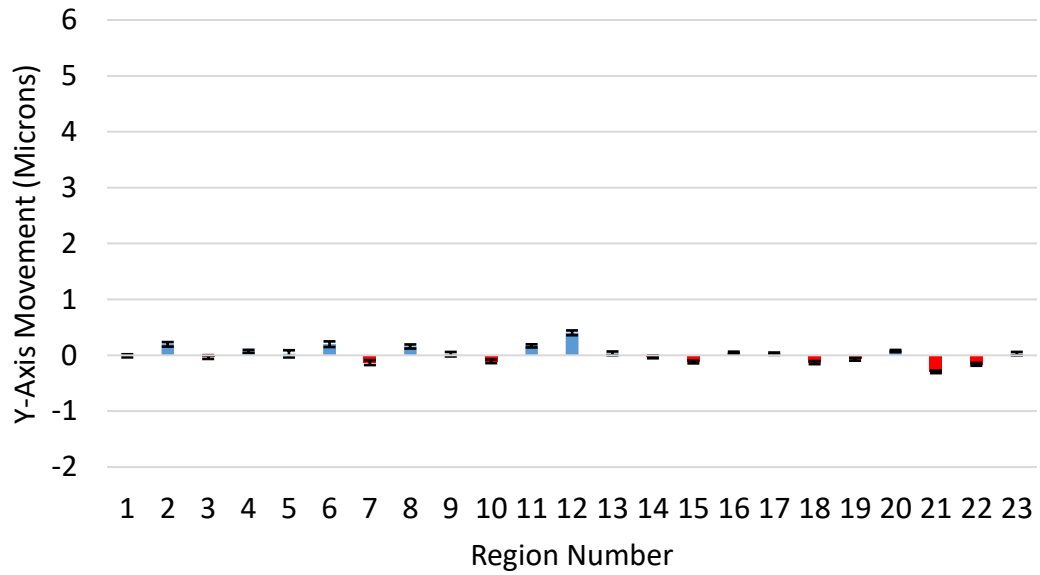


Figure 7b: This figure shows the same information as is present in Figure 7a, scaled to match Figure 8 for a better comparison between the magnitude of difference between control and experimental trials. Error bars are +/- 1 SEM.

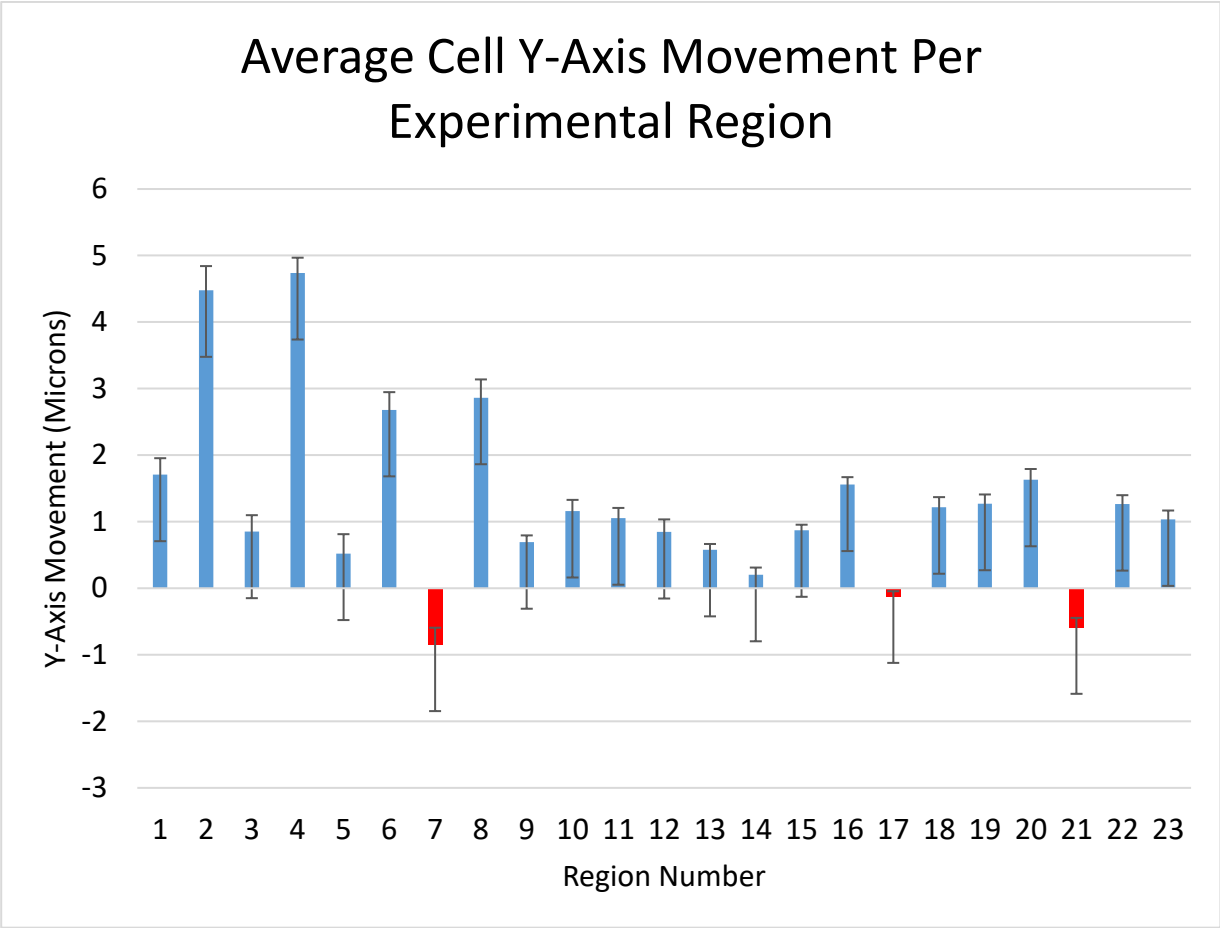


Figure 8: This graph shows the average cell movement along the Y-axis for each region of experimental trials, where L1-secreting cells are present. Positive values are taken to represent movement upwards, toward regions of high L1. Red bars indicate regions with average Y-movement in the negative range (net movement downward) Error bars are +/- 1 SEM.

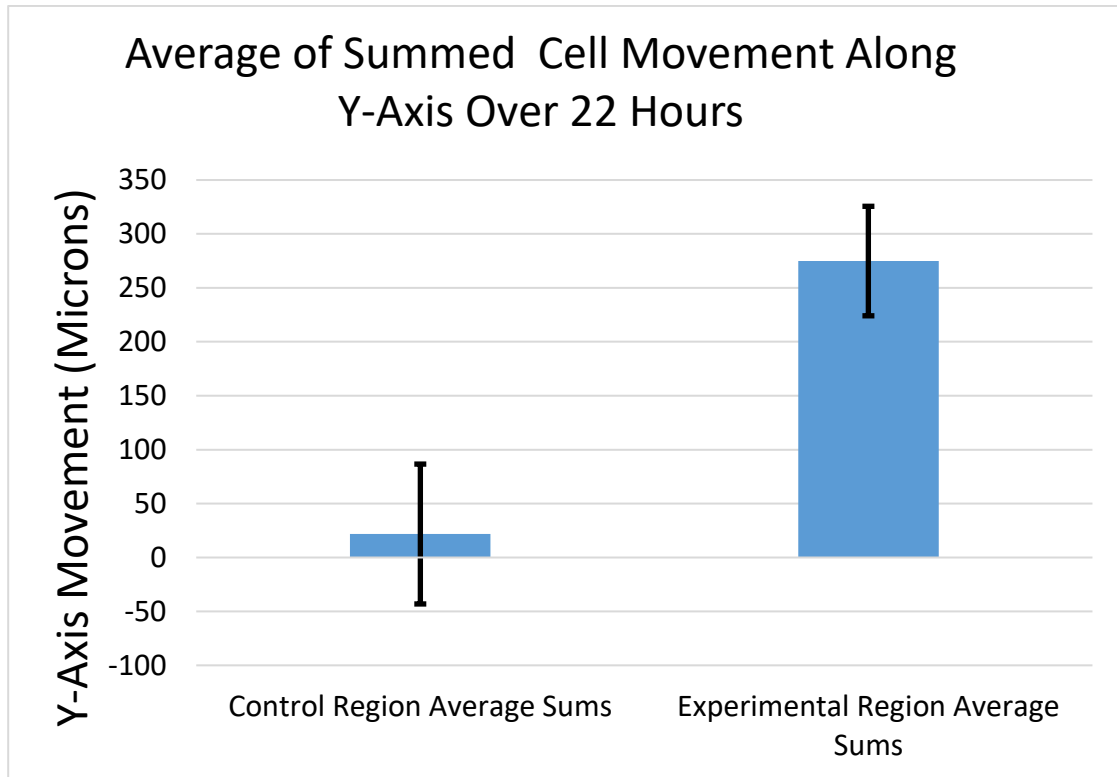


Figure 9a: The summed Y-movement value designated for all regions for each experimental condition (with L1-secreting cells vs without L1-secreting cells) were averaged. This graph compares the average of all regions' summed Y-movement between control and experimental conditions. The average shows a dramatic increase in positive movement in cells tracked in the presence of L1-secreting cells. Control SEM = +/- 64; Experimental SEM = +/- 51.

As GBM cells migrated outward from the edge of the bounded region, it was simple to qualitatively evaluate the general trend of the cells' directional movement. When L1-secreting cells were present, responding cells tended to move outward, and then begin migrating upward. When there were no L1-secreting cells present, the responding cells seemed to move more randomly or in looping patterns. I also found that migrating cells had a greater velocity in the presence of L1, as Anderson and

Galileo had found previously (2016). In general, when sources of L1ecto were present, cells moved an average of 33% faster.

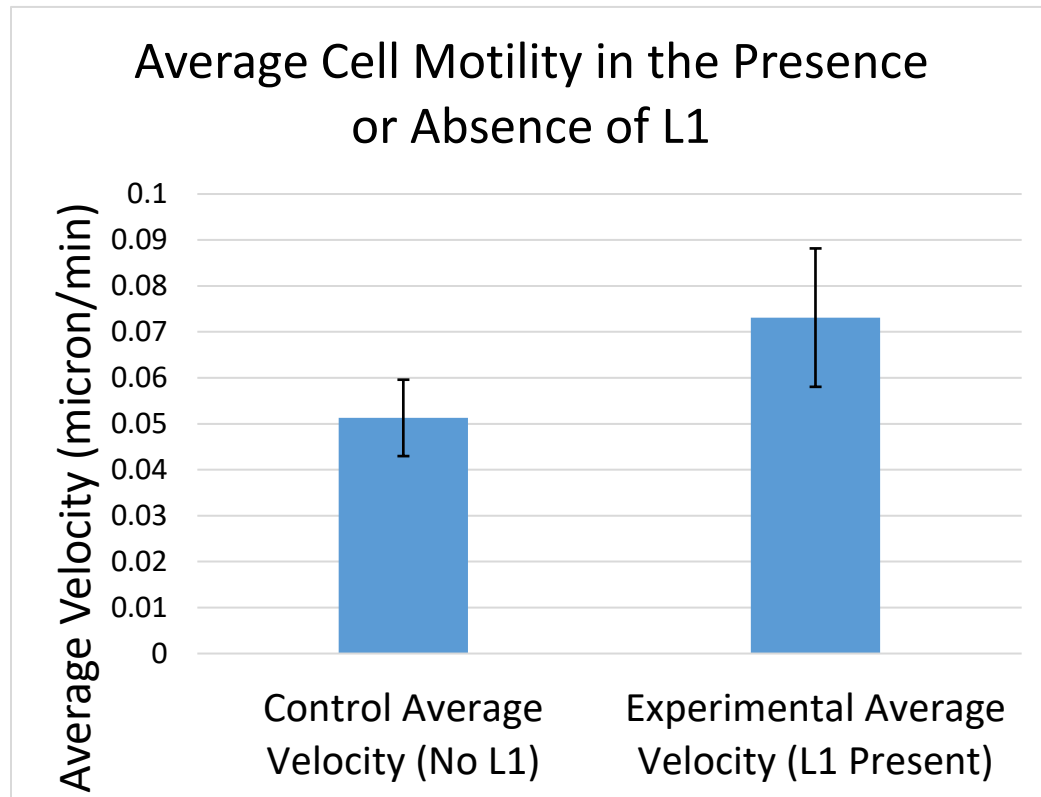


Figure 9b: In the presence of L1-secreting cells, L1-negative cells moved an average of 33% faster than cells that were not exposed to L1ecto. P-value >0.05, error bars are +/- 1 SEM.

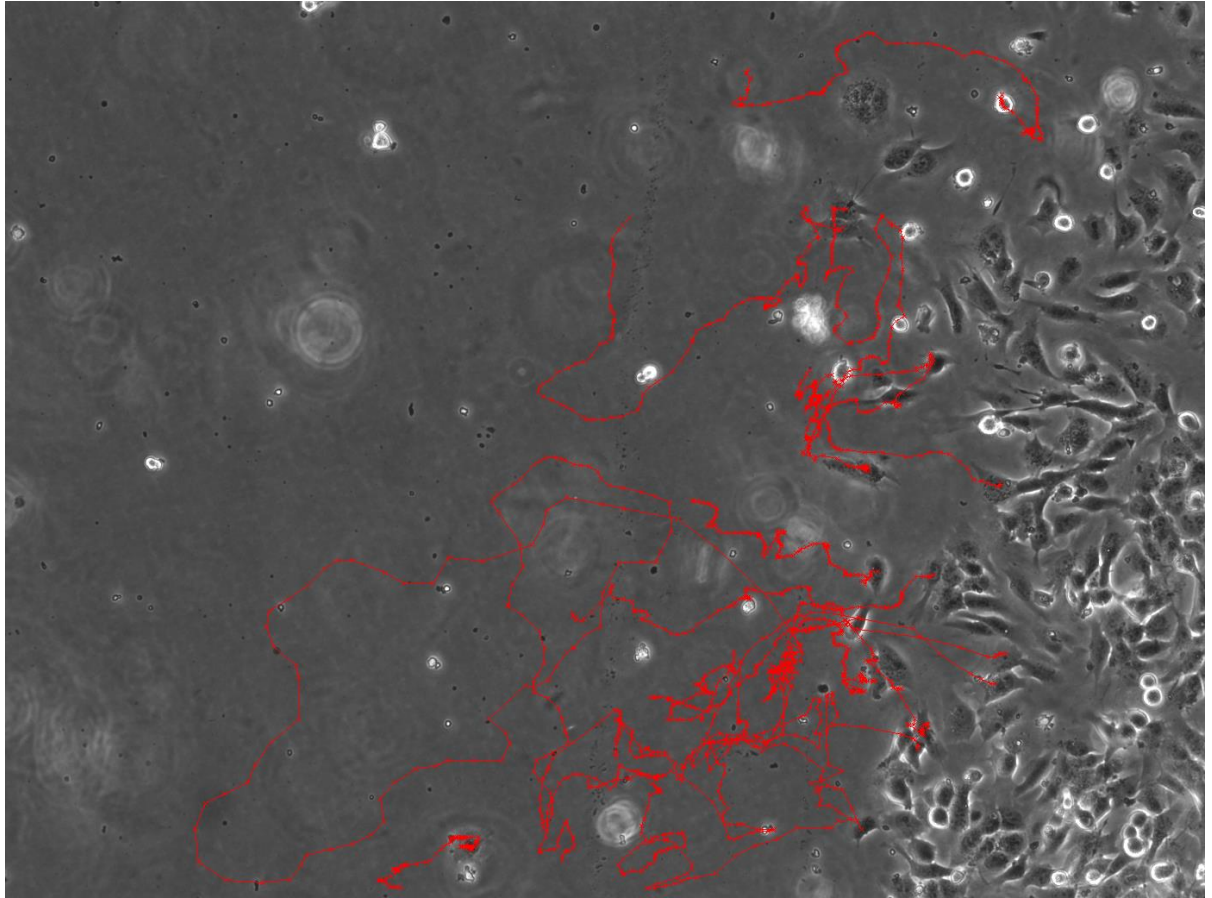


Figure 10: U-118/1879 cells along edge of bounded growth area. Control setup with no L1 secreting cells present. Image from time-point 1, with red lines indicating the path of cell movement over 22 hours.

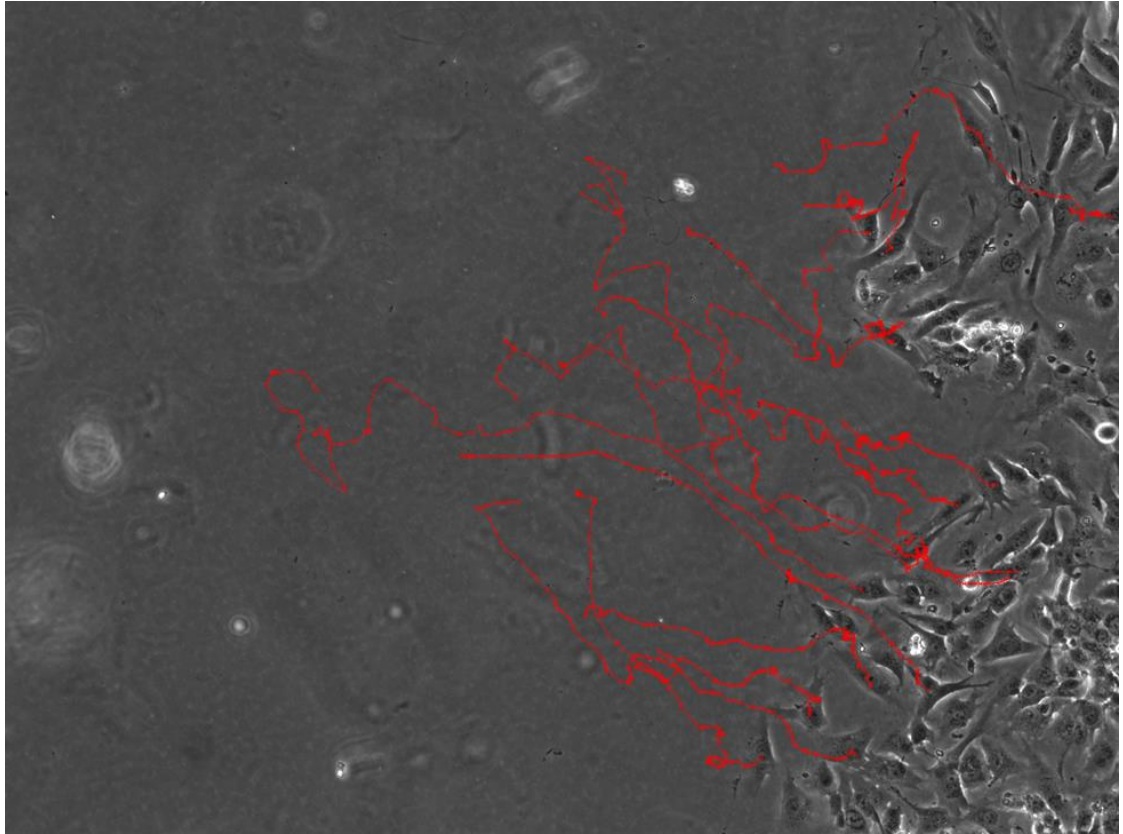


Figure 11: U-118/1879 cells along edge of bounded growth area. Experimental setup with L1 secreting cells present, grown vertically above the shown region. Image from time-point 1, with red lines indicating the path of cell movement over 22 hours.

These images (Fig 10, 11) are typical of their respective type of trial. For trials with L1-secreting cells present, not only was the average summed Y-movement much more positive than control trials, but each region had fewer occurrences of cells moving negatively, or away from regions of L1- secreting cells.

One observation of potential interest is that under both trial conditions, there appeared to be two phases of cell movement. It appeared that the cells would typically move more horizontally outward at first, and then move more vertically. This may be

elucidated by running a similar experimental design for a longer period of time. This may prove challenging, as attempts to run this setup longer for 24 hours often resulted in significant dehydration of the cells' environment, which caused the cells to die. There may be a way to plot increase in Y value over time, which would show that the increase in Y movement lags for a while.

A limitation of this experimental design was that any cell that was being tracked that moved out of the field of view could not be counted. This meant that in both experimental and control trials, some of the cells that moved the greatest amount were not tracked or analyzed. If they were able to be tracked, it may have affected my results. In the future there may be a way to track cells at a lower magnification so that the impact of this limitation could be reduced.

Another observation of note is that cells tracked on the edges of the bottom two regions (Regions 5 and 6 in Fig. 6) seemed to move slower and less directionally than the cells in the middle tier (Regions 4 and 5 in Fig. 6). This would make sense as the gradient of L1 would be expected to be less concentrated farther away from the secreting cells. However, as I was not able to accurately measure the distance of each region tracked from the secreting cells, I could not fully analyze this pattern. Preliminary analysis comparing the directional movement between middle tier and bottom tier regions did not show any significant difference between them. While a difference in the magnitude of directional movement at different distances from sources of L1ecto may make intuitive sense, it is likely that in this experimental design, the regions are too close together to witness any significant difference.

3.3 *In vivo* Results

Fluorescently labeled GBM cells were injected into the optic tecta of embryonic chicks, and their brains were fixed and Vibratome-sectioned 10 days later, immunostained for L1 and imaged by confocal microscopy. While there is no established rubric to quantify the relationship between visualized L1-secreting cells, L1-negative cells, and immunostained L1 molecules, qualitative observations are suggestive of a possible leader-follower relationship. It appeared that L1-negative cells were closely apposed to L1-secreting cells as they invaded the developing brain tissue, possibly along gradients of secreted L1 molecule or pathways laid down by L1-secreting cells (Fig 12b).

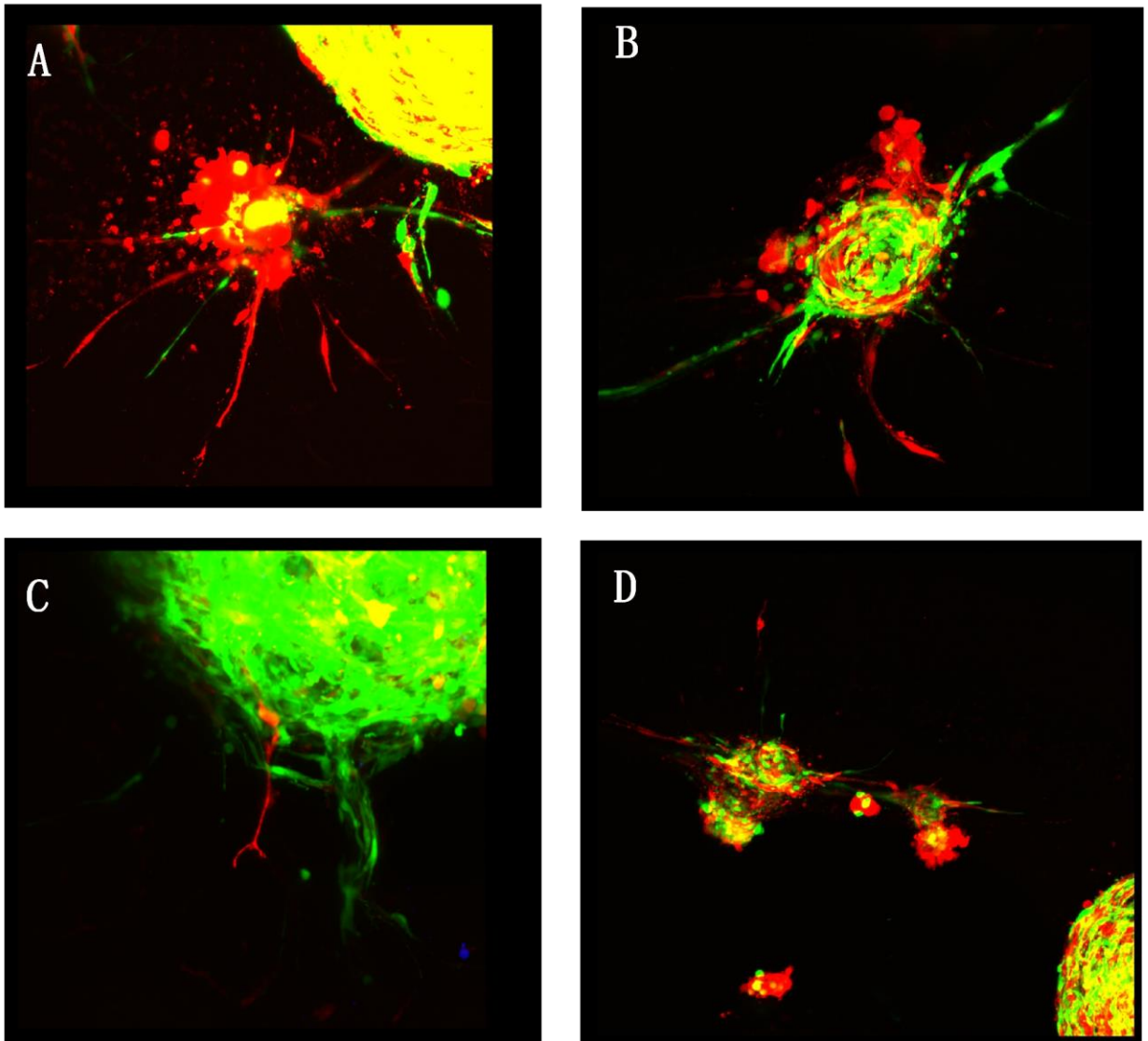


Figure 12a: Maximum projections of fluorescently labeled cells from a confocal z-stack of *In vivo* model control trial images. Chick brains were injected with a mixture of the same L1-negative GBM cell type, labelled with two different colors. Maximum projections of fluorescently labeled cells in a confocal z-stack. Virally labeled U-118/1879/mCherry (red), and U-118/1879/GFP (green). **A-C** imaged at 20x, **D** imaged at 10x.

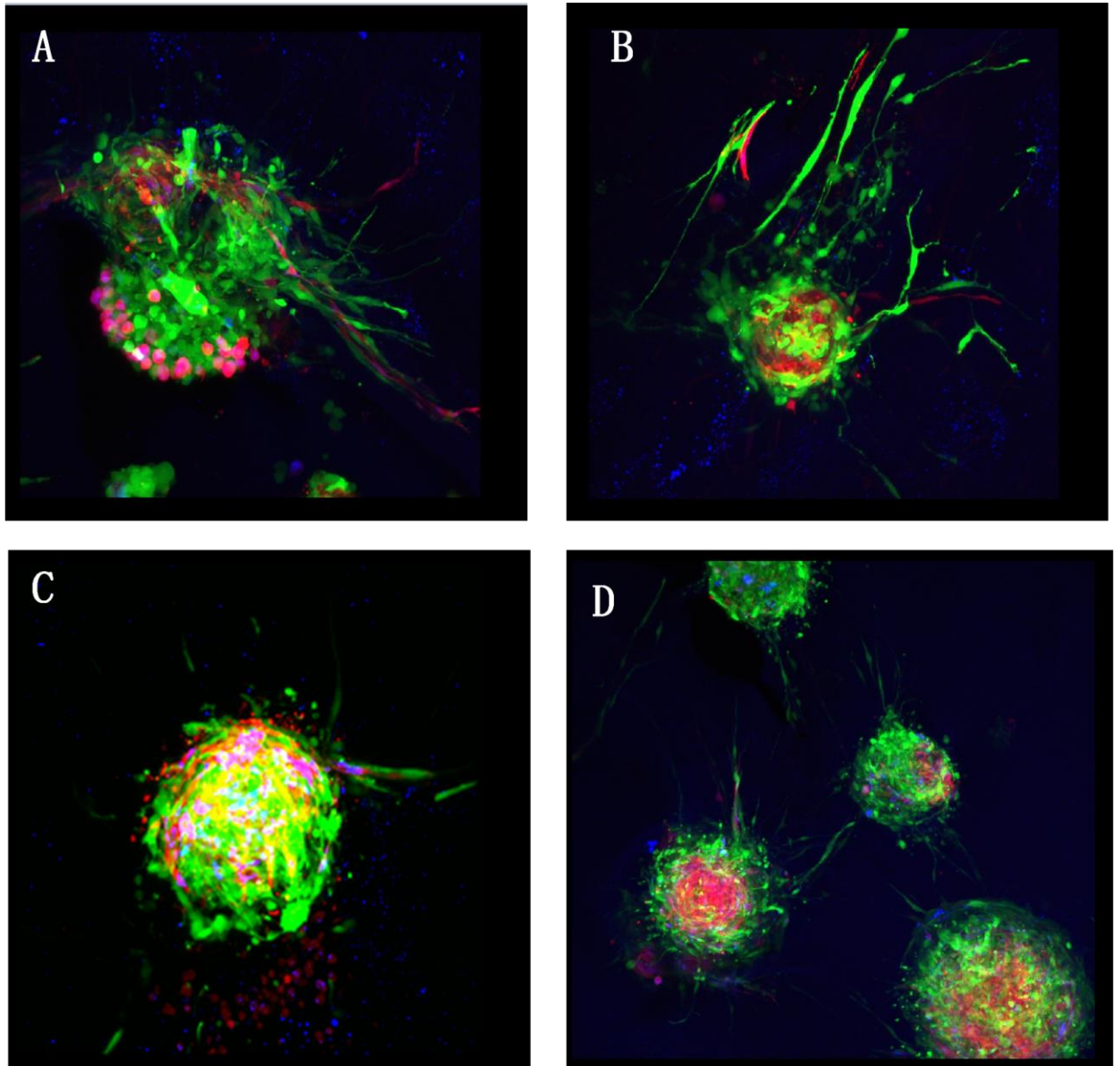


Figure 12b: Maximum projections of fluorescently labeled cells from a confocal z-stack of *In vivo* images under experimental conditions; mixture of L1-positive (red), and L1-negative (green) cells. Virally labeled U-118/L1LE/mCherry (red), U-118/1879/GFP (green), and immunostained L1 (blue). **A-C** imaged at 20x, **D** imaged at 10x.

When L1-secreting cells were present in the chick brain, the cancer tended to manifest as one large tumor mass with several smaller tumors surrounding the primary, or in a line leading from it. Tumors also tended to have many more outgrowths which usually consisted of L1-positive and L1-negative cells closely paired together.

When no L1 secreting cells were injected into the chick brain (i.e., only U-118/1879 cells), the tumors were generally smaller in size, with fewer satellite tumors. They also tended to have fewer outgrowths, and these outgrowths did not have close pairing of cells.

This difference in qualitative appearance between the experimental conditions, while not as straightforward or quantifiable as the *in vitro* trials, is suggestive of a chemotactic relationship between human GBM cells and L1; namely, that tumor cells that did not express L1 seem to have been affected by nearby cells that did produce L1 in both its membrane-bound and soluble forms via paracrine stimulation.

Chapter 4

Discussion

L1CAM has long been described as a permissive molecule that allows for the movement of neural cells (Schmid and Maness, 2008), but until now it has not been shown to have any chemotactic effect on cells of any type. My results suggest that cancer cells, specifically glioblastoma multiforme cell lines, do move directionally toward sources of proteolyzed, soluble L1 ectodomain, which may have far-reaching clinical significance. I showed that U-118 cells that do not express L1ecto will move directionally toward regions of high L1ecto concentration both *in vitro* and *in vivo*.

A potential limitation of this study is that only the U-118 GBM cell line established decades ago was used to test the chemotactic effect of soluble L1. U-118 cells were chosen because their relatively large cell body size and discrete movement pattern made them excellent candidates for time-lapse imaging. Other cells, such as the established T98G line, were experimented with, but I found that their small size and their pattern of motility were not congruent with clear tracking protocols at the magnification we desired (i.e., 10x magnification). Other GBM cell types should be tracked and analyzed with the same protocol to determine if the significant chemotactic effect of L1 we observed on U-118 cells is universal for all GBM cell types, and possibly other types of cancer as well. It would also be interesting to execute the same experiments with primary, recent patient derived tumor-cells to see if they behaved in the same way as well-established immortalized cell lines.

It is known that there is increased ADAM10 cleavage of L1 in many forms of human cancers (Maretzky et al., 2005), which drastically increases the concentration of soluble L1 protein present in the extracellular environment. This study's *in vitro* chemotaxis analysis showed that GBM cell lines responded to sources of secreted L1ecto most likely in a paracrine fashion. Cancer cells that have an increased production of soluble L1 may therefore act as beacons for surrounding cancer cells. This may explain, in part, why there is usually regrowth of tumor masses after surgical resection (Mallick et al., 2016) which contributes to the lethality of glioblastoma multiforme.

Other kinds of cancers are known to upregulate *LICAM* and have an increased presence of soluble L1. Breast cancer, in particular, has been shown to secrete proteolyzed L1 (Doberstein et al., 2014; Li and Galileo, 2010). It may yield interesting results if breast cancer cell lines were tracked with the same time-lapse microscopy protocol. If the chemotactic effect of L1 is universal for all cancer cells, this could greatly inform the course of research into molecular diagnostic criteria and molecular therapies for many forms of cancer.

Moving forward, using the chick optic tectum as an *in vivo* model to study the effects of L1 on tumor invasion will be an important tool. This study utilized the model as a reflection of our *in vitro* data that suggested a leader-follower relationship between L1-secreting cells and the responding L1-negative cells. My results showed a common trend of L1-negative cells closely following the paths of L1-secreting cells through the brain tissue, as well as seemingly increased overall invasion.

While my observations for this study were qualitative in nature, imaging of this kind could well be a source of valuable quantitative data. Numerically grading tumors

based on morphology has been a common practice in medicine since the 1950s, and the World Health Organization's criteria for grading tumors are still in use today (Muir and Percy, 1991). A point-scale rubric for rating the relative invasiveness of tumors with L1-secreting cells, versus tumors without L1-secreting cells, could be established based on visible morphological characteristics of the tumor masses. These characteristics could include factors such as the size of the main tumor, number of satellite tumors, number of tumor outgrowths, length of tumor outgrowths, distance between invading cells, depth of invading cell penetrance, etc. An established grading rubric for the invasiveness of GBM in chick brain could be a valuable tool when testing the efficacy of molecular inhibitors of L1 in an *in vivo* model. One of the limitations of the chick embryo model system is that cells are injected into the ventricle, where they greatly disperse. That results in multiple unknown points of adherence to the ventricular surface and, thus, invasion potentially from multiple points. Because of this random dispersal, one cannot be sure whether small tumors next to a large tumor, for instance, arose independently or whether they arose as outgrowths from the large tumor.

If L1-secreting cells do act as pathfinders for responding cancer cells via autocrine and paracrine signaling, it emphasizes the importance and potential utility of understanding molecular inhibitors of L1. Anderson and Galileo (2016) examined the interactions of small-molecule inhibitors of FGFR1, integrins, and FAK with L1. They found that these compounds significantly and specifically reduced the L1-mediated motility and proliferation of glioblastoma cells and may be viable as an adjuvant molecular therapy for patients with L1-positive tumors. This is especially true for cancers with a presence of soluble L1 due to ADAM10 cleavage. This study further

emphasizes the importance of researching potential molecular therapies to counteract L1, as sources of soluble L1 may be more related to tumor recurrence than previously thought. Rather than just stimulating cancer cells to reach farther into brain tissue at faster rates, tumor cells that secrete L1 may also be implicit as centralizers of new tumor masses forming from scattered cells after surgical resection.

REFERENCES

- Anderson, H. J., & Galileo, D. S. (2016). Small-molecule inhibitors of FGFR, integrins and FAK selectively decrease L1CAM-stimulated glioblastoma cell motility and proliferation. *Cellular Oncology*, 39(3), 229–242. <https://doi.org/10.1007/s13402-016-0267-7>
- Chang, S., Rathjen, F. G., & Raper, J. A. (1987). Extension of neurites on axons is impaired by antibodies against specific neural cell surface glycoproteins. *The Journal of Cell Biology*, 104(2), 355–362. Retrieved from <http://www.ncbi.nlm.nih.gov/pubmed/3543026>
- Conacci-Sorrell, M., Kaplan, A., Raveh, S., Gavert, N., Sakurai, T., & Ben-Ze'ev, A. (2005). The shed ectodomain of Nr-CAM stimulates cell proliferation and motility, and confers cell transformation. *Cancer Research*, 65(24), 11605–11612. <https://doi.org/10.1158/0008-5472.CAN-05-2647>
- Condeelis, J., Singer, R. H., & Segall, J. E. (2005). The Great Escape: When Cancer Cells Hijack the Genes for Chemotaxis and Motility. *Annu. Rev. Cell Dev. Biol*, 21, 695–718. <https://doi.org/10.1146/>
- Cretu, A., Fotos, J. S., Little, B. W., & Galileo, D. S. (2005). Human and rat glioma growth, invasion, and vascularization in a novel chick embryo brain tumor model. *Clinical & Experimental Metastasis*, 22, 225–236. <https://doi.org/10.1007/s10585-005-7889-x>
- De Bonis, P., Anile, C., Pompucci, A., Fiorentino, A., Balducci, M., Chiesa, S., ... Mangiola, A. (2013). The influence of surgery on recurrence pattern of glioblastoma. *Clinical Neurology and Neurosurgery*, 115(1), 37–43. <https://doi.org/10.1016/j.clineuro.2012.04.005>
- Doberstein, K., Milde-Langosch, K., Bretz, N. P., Schirmer, U., Harari, A., Witzel, I., ... Fogel, M. (2014). L1CAM is expressed in triple-negative breast cancers and is inversely correlated with Androgen receptor. *BMC Cancer*, 14(1), 958. <https://doi.org/10.1186/1471-2407-14-958>
- Faissner, A., Teplow, D. B., Kübler, D., Keilhauer, G., Kinzel, V., & Schachner, M. (1985). Biosynthesis and membrane topography of the neural cell adhesion molecule L1. *The EMBO Journal*, 4(12), 3105–3113. Retrieved from

<http://www.pubmedcentral.nih.gov/articlerender.fcgi?artid=554629&tool=pmcentrez&rendertype=abstract>

- Fotos, J. S., Patel, V. P., Karin, N. J., Temburni, M. K., Koh, J. T., & Galileo, D. S. (2006). Automated time-lapse microscopy and high-resolution tracking of cell migration. *Cytotechnology*, *51*(1), 7–19. <https://doi.org/10.1007/s10616-006-9006-7>
- Gutwein, P., Mechttersheimer, S., Riedle, S., Stoeck, A., Gast, D., Joumaa, S., ... Altevogt, P. (2003). ADAM10-mediated cleavage of L1 adhesion molecule at the cell surface and in released membrane vesicles. *The FASEB Journal*, *17*(2), 292–294. <https://doi.org/10.1096/fj.02-0430fje>
- Keilhauer, G., Faissner, A., & Schachner, M. (1985). Differential inhibition of neurone-neurone, neurone-astrocyte and astrocyte-astrocyte adhesion by L1, L2 and N-CAM antibodies. *Nature*, *316*(6030), 728–730. Retrieved from <http://www.ncbi.nlm.nih.gov/pubmed/4033770>
- Kiefel, H., Bondong, S., Hazin, J., Ridinger, J., Schirmer, U., Riedle, S., & Altevogt, P. (2012). L1CAM. *Cell Adhesion & Migration*, *6*(4), 374–384. <https://doi.org/10.4161/cam.20832>
- Koshihara, T., Hosotani, R., Miyamoto, Y., Ida, J., Tsuji, S., Nakajima, S., ... Imamura, M. (2000). Expression of stromal cell-derived factor 1 and CXCR4 ligand receptor system in pancreatic cancer: a possible role for tumor progression. *Clinical Cancer Research : An Official Journal of the American Association for Cancer Research*, *6*(9), 3530–3535. Retrieved from <http://www.ncbi.nlm.nih.gov/pubmed/10999740>
- Li, Y., & Galileo, D. S. (2010). Soluble L1CAM promotes breast cancer cell adhesion and migration in vitro, but not invasion. *Cancer Cell International*, *10*(1), 34. <https://doi.org/10.1186/1475-2867-10-34>
- Liljelund, P., Ghosh, P., & van den Pol, A. N. (1994). Expression of the neural axon adhesion molecule L1 in the developing and adult rat brain. *The Journal of Biological Chemistry*, *269*(52), 32886–32895. Retrieved from <http://www.ncbi.nlm.nih.gov/pubmed/7806515>
- Lindner, J., Rathjen, F. G., & Schachner, M. (1983). L1 mono- and polyclonal antibodies modify cell migration in early postnatal mouse cerebellum. *Nature*, *305*(5933), 427–430. <https://doi.org/10.1038/305427a0>
- Mallick, S., Benson, R., Hakim, A., & Rath, G. K. (2016). Management of glioblastoma after recurrence: A changing paradigm. *Journal of the Egyptian*

National Cancer Institute, 28(4), 199–210.
<https://doi.org/10.1016/J.JNCI.2016.07.001>

- Maretzky, T., Schulte, M., Ludwig, A., Rose-John, S., Blobel, C., Hartmann, D., ... Reiss, K. (2005). L1 Is Sequentially Processed by Two Differently Activated Metalloproteases and Presenilin/ -Secretase and Regulates Neural Cell Adhesion, Cell Migration, and Neurite Outgrowth. *Molecular and Cellular Biology*, 25(20), 9040–9053. <https://doi.org/10.1128/MCB.25.20.9040-9053.2005>
- Mohanan, V., Temburni, M. K., Kappes, J. C., & Galileo, D. S. (2013). L1CAM stimulates glioma cell motility and proliferation through the fibroblast growth factor receptor. *Clinical & Experimental Metastasis*, 30(4), 507–520. <https://doi.org/10.1007/s10585-012-9555-4>
- Moos, M., Tacke, R., Scherer, H., Teplow, D., Früh, K., & Schachner, M. (1988). Neural adhesion molecule L1 as a member of the immunoglobulin superfamily with binding domains similar to fibronectin. *Nature*, 334(6184), 701–703. <https://doi.org/10.1038/334701a0>
- Muir, C. S. and P. C. (1991). Chapter 7 . Classification and coding of neoplasms, (Icd), 64–81. Retrieved from <https://www.iarc.fr/en/publications/pdfs-online/epi/sp95/sp95-chap7.pdf>
- Ponten, J., & Westermark, B. (1978). Properties of Human Malignant Glioma Cells In Vitro. *Medical Biology*, 56, 184–193. Retrieved from [https://sakai.udel.edu/access/content/group/085e2828-3da8-43e7-ae23-481410ecda4f/Glioma Papers/Ponten and Westermark 1978.pdf](https://sakai.udel.edu/access/content/group/085e2828-3da8-43e7-ae23-481410ecda4f/Glioma%20Papers/Ponten%20and%20Westermark%201978.pdf)
- Roussos, E. T., Condeelis, J. S., & Patsialou, A. (2011). Chemotaxis in cancer. *Nature Reviews. Cancer*, 11(8), 573–587. <https://doi.org/10.1038/nrc3078>
- Schmid, R. S., & Maness, P. F. (2008). L1 and NCAM adhesion molecules as signaling coreceptors in neuronal migration and process outgrowth. *Current Opinion in Neurobiology*, 18(3), 245–250. <https://doi.org/10.1016/j.conb.2008.07.015>
- Scotton, C. J., Wilson, J. L., Scott, K., Stamp, G., Wilbanks, G. D., Fricker, S., ... Balkwill, F. R. (2002). Multiple actions of the chemokine CXCL12 on epithelial tumor cells in human ovarian cancer. *Cancer Research*, 62(20), 5930–5938. Retrieved from <http://www.ncbi.nlm.nih.gov/pubmed/12384559>
- Smoll, N. R., Schaller, K., & Gautschi, O. P. (2013). Long-term survival of patients with glioblastoma multiforme (GBM). *Journal of Clinical Neuroscience*, 20(5), 670–675. <https://doi.org/10.1016/j.jocn.2012.05.040>

- Swaney, K. F., Huang, C.-H., & Devreotes, P. N. (2010). Eukaryotic Chemotaxis: A Network of Signaling Pathways Controls Motility, Directional Sensing, and Polarity. *Annual Review of Biophysics*, 39(1), 265–289. <https://doi.org/10.1146/annurev.biophys.093008.131228>
- Wang, W., Wyckoff, J. B., Goswami, S., Wang, Y., Sidani, M., Segall, J. E., & Condeelis, J. S. (2007). Coordinated Regulation of Pathways for Enhanced Cell Motility and Chemotaxis Is Conserved in Rat and Mouse Mammary Tumors. *Cancer Res*, 67(8), 3505–3511. <https://doi.org/10.1158/0008-5472.CAN-06-3714>
- Wen, P. Y., & Kesari, S. (2008). Malignant Gliomas in Adults. *New England Journal of Medicine*, 359(5), 492–507. <https://doi.org/10.1056/NEJMra0708126>
- Yang, M., Li, Y., Chilukuri, K., Brady, O. A., Boulos, M. I., Kappes, J. C., & Galileo, D. S. (2011). L1 stimulation of human glioma cell motility correlates with FAK activation. *Journal of Neuro-Oncology*, 105(1), 27–44. <https://doi.org/10.1007/s11060-011-0557-x>
- Yang, M., Li, Y., Kalyani, @bullet, @bullet, C., Brady, O. A., Magdy, @bullet, ... Kappes, J. C. (n.d.). L1 stimulation of human glioma cell motility correlates with FAK activation. *J Neurooncol*. <https://doi.org/10.1007/s11060-011-0557-x>

Appendix A

TRIAL AND ERROR IN DEVELOPING PROTOCOLS

A.1 Chemotaxis Assay Prototypes

Much of this research was dedicated to developing a chemotaxis assay that was accurate, inexpensive, and reproducible. There were many prototypic incarnations of my experimental protocols before the custom cell culture dish described in Fig. 4 and its associated protocol were established. In the interest of continuing this line of research, this appendix details the ineffective versions of the chemotaxis assay so that they may not be repeated.

A.1.1 Chemotaxis Plate Version 1 “The Double Ring”

The first form of time-lapse assay that I attempted was meant to analyze the velocity of cells grown in the presence of L1-producing cells, and it utilized the mouth of a 15 mL centrifuge tube removed via hacksaw. The factory-perfect edge of the tube was adhered to the center of a cell culture dish with rubber cement. This created “inner circle” and “outer circle” regions for cells to be plated. L1 producing cells were plated on the inner circle, and L1-negative cells were grown on the outer circle. After a day of growth, the inner circle was removed with sterilized forceps and cells along the edge of the outer circle were tracked as they moved inward. The velocities of these cells were compared to cells grown in the same setup, but with non L1 producing cells grown in the inner circle.

The main flaw of this experimental design was that due to the orientation of the regions to each other, it was impossible to gain useful data on the directionality of the cells' movement – it was only useful for gathering information on L1's effect on cell velocity, which had already been shown by previous research. Another flaw of this design was that the removal of the inner circle boundary left large regions of rubber cement residue. Cells seemed adverse to the residue and either would not proceed to move forward over it, or would do so very slowly, which compromised the velocity data we were gathering. It also led us to question whether the rubber cement was toxic to the cells and as such would be a potential confounding variable.

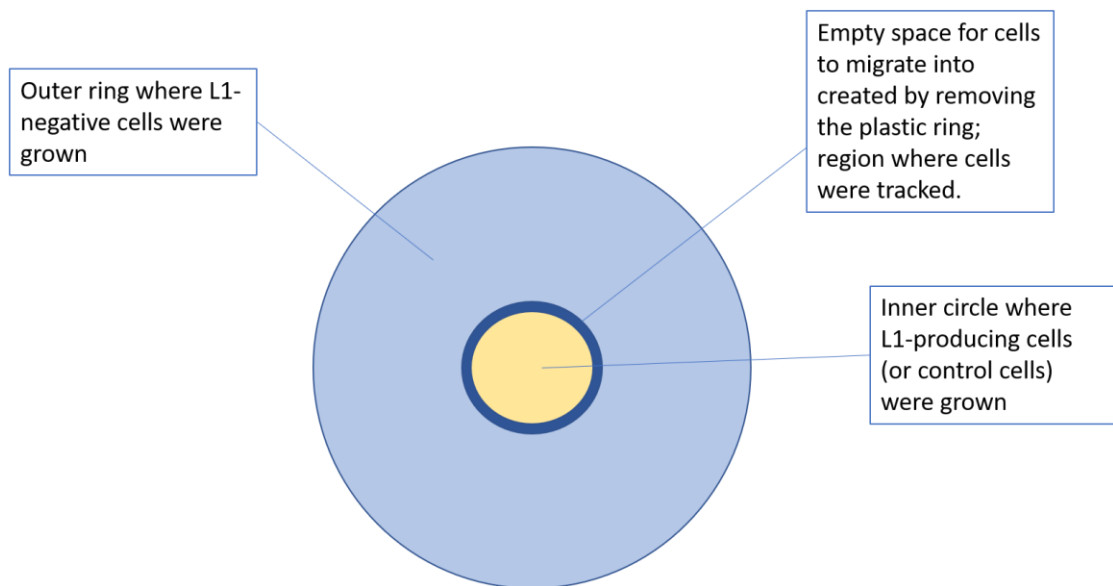


Figure 13: First attempt at designing a modified chemotaxis assay plate. L1-negative cells were grown in outer region of plate, while L1-secreting cells were grown for 24 hours inside the bounded inner circle created from adhering the mouth of a 15mL plastic tube with rubber cement. Once removed, the area where the tube had been became the space where responding cells' movement was tracked with time-lapse microscopy.

A.1.2 Chemotaxis Plate Version 2 “Diamond of Rings”

This version did not address the issues with the rubber cement, but it focused on finding a design that could give us meaningful data on the directionality of the cells' movement. The design included four of the 15 mL tube tops attached via rubber cement in a diamond shaped pattern. The plan was to track cells migrating from the top and bottom regions and see if they would move preferentially toward the left region (containing L1 producing cells) or the right (containing L1-negative cells). It was during these trials that I realized the poor design element introduced by using rubber cement and I decided to throw out the data of the current and previous trials and create a new design that was not reliant on the rubber cement as an adhesive.

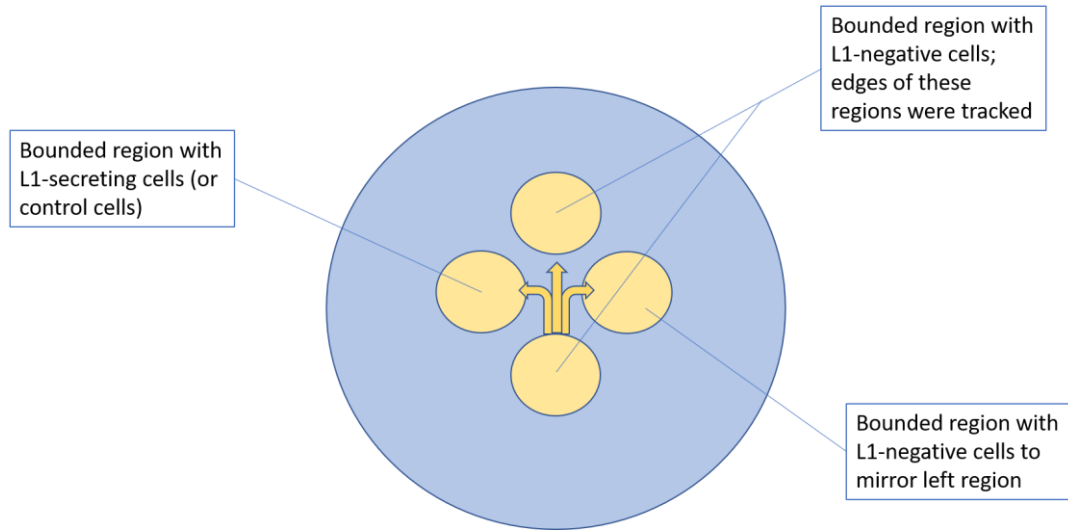


Figure 14: The second chemotaxis plate prototype involved using rubber cement to adhere four plastic rings in a diamond-shape pattern. No cells were grown in what would be considered “the outer ring” in the previous experimental setup. Arrows indicate the potential movement of cells.

A.1.3 Chemotaxis Plate Version 3 “The Krillin Plate”

It was at this point that I started using the hydrophobic adhesive tape that I would use in the final experimental design. Trials with the tape showed that it left little to no residue, and cells grown on regions where tape was applied and removed grew and moved normally. This design was very similar in construction to the final version we used, but instead of six, 1cm square regions, I used a standard hole punch to create six circular regions for cells to be grown within. Like in the final version of the experimental design, the top two regions contained L1-secreting cells (or L1-negative cells for control trials), while the other four regions contained L1-negative responding cells. Early trials using this format were promising, but I realized that having our

bounded regions have a flat edge would lead to more consistent, reliable data and be closer in design to scratch assays. As such I modified this design to my current model, as previously described in the methods section, and in Figure 6 in the results section.

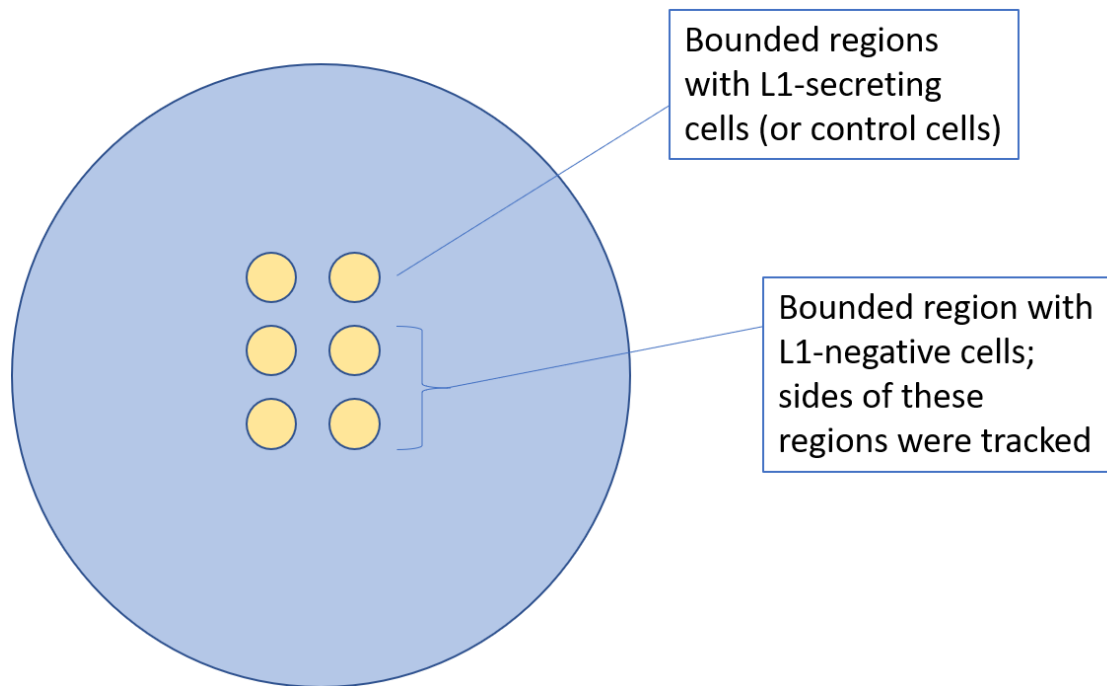


Figure 15: The penultimate experimental design for the chemotaxis plate; pilot experiments using this design yielded encouraging results, but I decided that having a square border would be more consistent.

A.1.4 *In vitro* images Used

Figure 10 uses an image from my 3/14/18 time-lapse experiment at region 1.

Figure 11 uses an image from my 9/15/17 time-lapse experiment at region 6.

A.2 *In vivo* Design

Just as developing successful protocols for the *in vitro* portions of this research was a learning process, the methods I employed for my *in vivo* experiments involved trial and error to find a consistent, economical, and reproducible format.

A.2.1 Vital dyes vs. viral labeling

Early experiments utilizing chick brain as an *in vivo* model used vital dye labeled cells rather than viral labeling. GBM cells were incubated in either Vybrant DiI and Vybrant DiO (Thermo Fisher Scientific) to label them prior to injection. While this resulted in quality images, I was concerned about the longevity of the labeling. Because these vital dyes are lipophilic and result in labeling changing from even membrane staining to puncta in cell cytoplasm, they were inherently a diffusible labeling system. I was concerned that over the course of the 10 days of growth and cell division, I was only seeing a fraction of the total number of cells present that may have been too weakly labeled to visualize. I decided that viral labeling would be a better option for continued use *in vivo* because of its non-diluting nature of labeling

A.2.2 Slide construction version 1

When mounting sections of chick brain onto slides for imaging, because tissue sections were 350 microns thick, the cover glass needed to be elevated in some way to prevent the section from being crushed. I initially laid 2 layers of standard 170-micron electrical tape in parallel strips on the edges of where the cover glass would rest. This was effective in preventing the tissue from being crushed, but I could not seal the cover glass with nail polish to prevent dehydration of the section. Early attempts to do so resulted in the nail polish bleeding into the mounting media and obscuring the

tissue section. Therefore my early slides would expire in a shorter time frame than I would have wanted.

To address this issue, I began using 1” wide electrical tape of the same standard thickness to cover the entirety of the slide, with a 1cm square region removed from the center for the specimen to be mounted. This is the current design used by the lab.

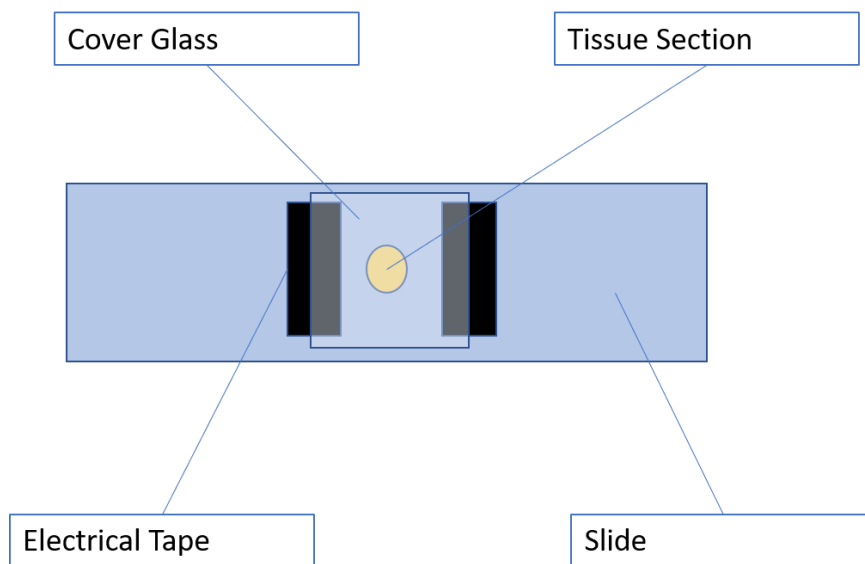


Figure 16: The first version of my slides for mounting 350-micron tissue sections. This design was effective for preventing tissue sections from being crushed, but it was impossible to seal with nail polish which prevented preservation of the slides for future use.

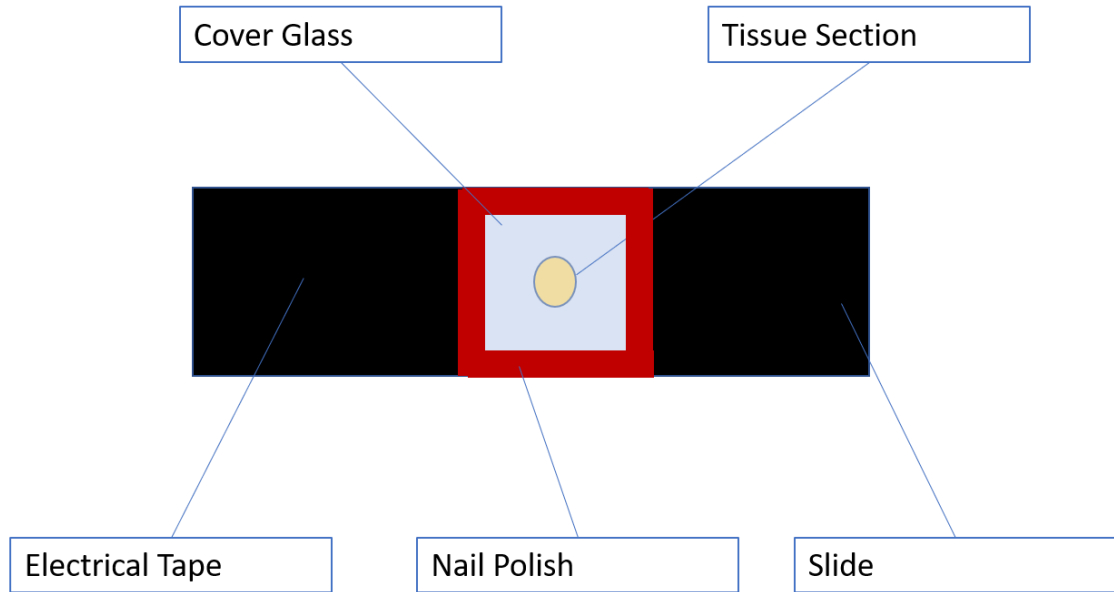


Figure 17: The second iteration of my slide design for mounting 350-micron tissue sections. By having the entire area around the specimen elevated with electrical tape, I was able to seal the cover glass with nail polish in order to preserve the slide for future use.

A.2.3 *In vitro* images used

For Figure 12a:

Legend designation	Date of injection	Slide number
A	3/2/18	#15B1, 20x #1
B	3/2/18	#15B2, 20x #1
C	7/17/17	#16B, 20x #1
D	3/2/18	#15B1, 10x #1

For Figure 12b:

Legend designation	Date of injection	Slide number
A	1/23/18	#8B1, 20x #1
B	1/23/18	#8B1, 20x, #2

C	7/17/17	#7A, 10x #1
D	1/23/18	#9B2, 20x #1